Numerical Methods for the Generalized Zakharov System

Weizhu Bao[a*], *Fangfang Sun*[a], *G.W. Wei*[b †]

[a]Department of Computational Science

National University of Singapore, Singapore 117543, Singapore

[b]Department of Mathematics

Michigan State University, East Lansing, MI 48824, USA

Abstract

We present two numerical methods for the approximation of the generalized Zakharov system (ZS). The first one is the time-splitting spectral (TSSP) method, which is explicit, time reversible and time transverse invariant if the generalized ZS is, keeps the same decay rate of the wave energy as that in the generalized ZS, gives exact results for the plane-wave solution, and is of spectral-order accuracy in space and second-order accuracy in time. The second one is to use a local spectral method, the discrete singular convolution (DSC) for spatial derivatives and the fourth-order Runge-Kutta (RK4) for time integration, which is of high (the same as spectral) order accuracy in space and can be applied to deal with general boundary conditions. In order to test accuracy and stability, we compare these two methods with other existing methods: Fourier pseudospectral method (FPS) and wavelet-Galerkin method (WG) for spatial derivatives combining with the RK4 for time integration, as well as the standard finite difference method (FD) for solving the ZS with a solitary-wave solution. Furthermore, extensive numerical tests are presented for plane waves, solitary-wave collisions in 1d, as well as a 2d problem of the generalized ZS. Numerical results show that TSSP and DSC

*Email address: bao@cz3.nus.edu.sg. Fax: 65-67746756

†Email address: wei@math.msu.edu. Fax: 517-4321562

are spectral-order accuracy in space and much more accurate than FD, and for stability, TSSP requires $k = O(h)$, DSC-RK4 requires $k = O(h^2)$ for fixed acoustic speed, where k is the time step and h is the spatial mesh size.

1 Introduction

The specific problem we study numerically is the generalized Zakharov system (ZS) describing the propagation of Langmuir waves in plasma with a plasma envelope.

$$i\,E_t + \Delta\,E - \alpha N\,E + \lambda|E|^2\,E + i\gamma\,E = 0, \qquad \mathbf{x} \in \mathbb{R}^d, \quad t > 0, \tag{1.1}$$

$$\varepsilon^2 N_{tt} - \Delta(N - \nu|E|^2) = 0, \qquad \mathbf{x} \in \mathbb{R}^d, \quad t > 0, \tag{1.2}$$

$$E(\mathbf{x},0) = E^0(\mathbf{x}),\ N(\mathbf{x},0) = N^0(\mathbf{x}),\ N_t(\mathbf{x},0) = N^{(1)}(\mathbf{x}), \quad \mathbf{x} \in \mathbb{R}^d; \tag{1.3}$$

where the complex unknown function $E(\mathbf{x},t)$ is the slowly varying envelope of the highly oscillatory electric field, the real unknown function $N(\mathbf{x},t)$ is the deviation of the ion density from its equilibrium value, ε is a parameter inversely proportional to the acoustic speed, $\gamma \geq 0$ is a damping parameter, and α, λ, ν are all real parameters. The generalized ZS is time reversible and time transverse invariant if $\gamma = 0$ in (1.1).

The general form of (1.1), (1.2) covers many generalized Zakharov systems arising in various physical applications. For example, when $\varepsilon = 1$, $\nu = -1$, $\lambda = 0$, $\gamma = 0$ and $\alpha = 1$, the system of Eqs. (1.1) and (1.2) reduces to the well-known Zakharov system (ZS), which has been first derived by Zakharov [47] to describe the interaction between Langmuir (dispersive) and ion acoustic (approximately nondispersive) waves in a plasma. Later, it has become commonly accepted that the ZS is a general model to govern interaction of dispersive and nondispersive waves. Neither the standard ZS is integrable [33], nor the generalized ZS (1.1), (1.2). When $\varepsilon = 1$, $\nu = -1$ and $\lambda \neq 0$, a cubic nonlinearity is added to the first equation (1.1). When $\gamma > 0$, a linear damping term is added to the ZS. When $\varepsilon \to 0$ (corresponding to infinite acoustic speed or 'subsonic limit') in (1.2), one gets $N = \nu|E|^2$, which together with (1.1), leads to the well-known nonlinear Schrödinger equation (NLS) without ($\gamma = 0$) or with ($\gamma > 0$) a linear damping term:

$$i\,E_t + \Delta\,E + (\lambda - \alpha\nu)|E|^2\,E + i\gamma\,E = 0, \qquad \mathbf{x} \in \mathbb{R}^d, \quad t > 0.$$

The global existence of weak solutions of the Zakharov equations in 1d is provided in [36], and existence and uniqueness of smooth solutions for the equations are obtained provided that smooth initial data are prescribed. The wellposedness of the ZS has recently improved in [11] for $d = 1, 2, 3$, and extended for the case with generalized nonlinearity [15].

Numerical methods for the standard Zakharov system, i.e. $\varepsilon = 1$, $\nu = -1$, $\lambda = 0$, $\gamma = 0$ in (1.1) and (1.2), were studied in the last two decades. Payne et al. [28] proposed a Fourier spectral method for the 1d Zakharov system. They used

only two-thirds of the Fourier components for a particular mesh in the fast Fourier transform in order to suppress the aliasing errors in their algorithm [28]. Of course, this is not an optimal way to use the spectral method. In [18, 19], Glassey presented an energy-preserving implicit finite difference scheme for the system and proved its convergence. Later, Chang et al. [13] considered an implicit or semiexplicit conservative finite difference scheme for the ZS, proved its convergence, and extended their method for the generalized Zakharov system [14]. One can find more numerical study of soliton-soliton collisions in a (generalized) Zakharov system in [27, 23, 24].

The goal of this paper is to design new and efficient numerical methods for the generalized ZS (1.1), (1.2) with spectral spatial accuracy and persevering the physical property of the generalized ZS at the discretized level. To this end, we propose a time-splitting spectral (TSSP) approximation and a discrete singular convolution (DSC) algorithm for the generalized Zakharov system. TSSP is explicit, time reversible and time transverse invariant if the generalized ZS (1.1), (1.2) is, easy to extend to high dimensions, and gives exact results for plane-wave solutions of the ZS. For stability, TSSP requires $k = O(h)$. In fact, the spectral method has showed greatly success in solving problems arising from many areas [20, 12] and the split-step procedure was presented for differential equations [35] and applied for Schrödinger equation [26, 38, 17] and KDV equation [39]. Recently, the time-splitting spectral approximation was used and studied for NLS equation in the semiclassical regimes in [7, 8] and applied to the numerical study of the dynamics of Bose-Einstein condensation [6, 5] as well as for NLS under nonzero far-field conditions [4]. Very promising numerical results were obtained due to its exponentially high order accuracy in space and persevering the physical property of NLS at the discretized level. The approach for the ZS is based on a time splitting for (1.1) which keeps the same decay rate in time of the wave energy $\int_{\mathbb{R}^d} |E(x,t)|^2\, dx$ as that in (1.1) and (1.2). In [9], the first two authors extend the TSSP for discretizing the vector Zakharov system (VZS) for multi-component plasma and studying numerically the convergence of generalized ZS to NLS in the 'subsonic limit' and simulating a 3d vector ZS.

The discrete singular convolution (DSC) has recently been proposed by Wei [41] as a local spectral method for the numerical discretization of spatial derivatives. The main merit of DSC is that it is of spectral accuracy for approximating derivatives and can be applied to deal with complex geometries and general boundary conditions. The method was successfully applied to solve many science and engineering problems, including eigenvalue problems [43] of both quantum and classical origins, analysis of stochastic process [41, 42], simulation of fluid flows in simple and complex geometries [40], vibration analysis of solid structures [44], electromagnetic wave propagation [34], and nanoscale pattern formation in a circular domain [22]. The mathematical foundation of this algorithm is the theory of distributions [32]. Numerical analysis indicates that the DSC method has spectral convergence for approximating appropriate functions [3]. We compare the accuracy, stability of TSSP and DSC with other existing methods like finite difference methods. Numerical results demonstrate the high accuracy and efficiency of the two proposed methods for

the ZS.

The paper is organized as follows. In section 2 we present the time-splitting spectral discretization and DSC algorithm of the generalized Zakharov system. In section 3 we compare the accuracy and stability of different methods for the ZS with a solitary wave solution, as well as present numerical results for plane waves, soliton-soliton collisions in 1d and a 2d problem of the generalized ZS. In section 4 we draw some conclusions.

2 Numerical methods

In this section we present time-splitting spectral discretizations and DSC algorithm for the generalized ZS (1.1), (1.2), and (1.3) with periodic boundary conditions. For simplicity of notation we shall introduce the method in one space dimension ($d = 1$). Generalizations to $d > 1$ are straightforward for tensor product grids and the results remain valid without modifications. For $d = 1$, the problem becomes

$$i\,E_t + E_{xx} - \alpha N\,E + \lambda|E|^2\,E + i\gamma\,E = 0, \qquad a < x < b, \quad t > 0, \tag{2.1}$$

$$\varepsilon^2 N_{tt} - (N - \nu\,|E|^2)_{xx} = 0, \qquad a < x < b, \quad t > 0, \tag{2.2}$$

$$E(x,0) = E^0(x),\ N(x,0) = N^0(x),\ N_t(x,0) = N^{(1)}(x), \quad a \le x \le b, \tag{2.3}$$

$$E(a,t) = E(b,t), \qquad E_x(a,t) = E_x(b,t), \qquad t \ge 0, \tag{2.4}$$

$$N(a,t) = N(b,t), \qquad N_x(a,t) = N_x(b,t), \qquad t \ge 0. \tag{2.5}$$

Moreover, we supplement (2.1)-(2.5) by imposing the compatibility condition

$$E^0(a) = E^0(b), \quad N^0(a) = N^0(b), \quad N^{(1)}(a) = N^{(1)}(b), \quad \int_a^b N^{(1)}(x)\,dx = 0. \tag{2.6}$$

As is well known, the generalized ZS has the following property

$$D(t) = \int_a^b |E(x,t)|^2\,dx = e^{-2\gamma t}\int_a^b |E^0(x)|^2\,dx = e^{-2\gamma t}D(0), \qquad t \ge 0; \tag{2.7}$$

where D is called as the wave energy of the generalized ZS. When $\gamma = 0$, $D(t) \equiv D(0)$, i.e., it is an invariant of the ZS [13]. Furthermore, the ZS also has the following properties

$$\int_a^b N_t(x,t)\,dx = 0, \qquad \int_a^b N(x,t)\,dx = \int_a^b N^0(x)\,dx = \text{const.}, \qquad t \ge 0. \tag{2.8}$$

In some cases, the boundary conditions (2.4) and (2.5) may be replaced by

$$E(a,t) = E(b,t) = 0, \qquad N(a,t) = N(b,t) = 0, \qquad t \ge 0. \tag{2.9}$$

We choose the spatial mesh size $h = \Delta x > 0$ with $h = (b-a)/M$ for M being an even positive integer, the time step being $k = \Delta t > 0$ and let the grid points and the time step be

$$x_j := a + j\ h, \qquad t_m := m\ k, \qquad j = 0, 1, \cdots, M, \qquad m = 0, 1, 2, \cdots.$$

Let E_j^m and N_j^m be the approximations of $E(x_j, t_m)$ and $N(x_j, t_m)$, respectively. Furthermore, let E^m and N^m be the solution vector at time $t = t_m = mk$ with components E_j^m and N_j^m, respectively.

2.1 Time-splitting spectral discretizations (TSSP)

From time $t = t_m$ to $t = t_{m+1}$, the second equation (2.2) in the generalized ZS is discretized by Fourier spectral method in space and second-order central difference scheme in time, and the first equation (2.1) is solved in two splitting steps. One solves first

$$i\ E_t + E_{xx} = 0, \tag{2.10}$$

for the time step of length k, followed by solving

$$i\ E_t = \alpha N\ E - \lambda |E|^2\ E - i\gamma\ E, \tag{2.11}$$

for the same time step. Equation (2.10) will be discretized in space by the Fourier spectral method and integrated in time *exactly*. For $t \in [t_m, t_{m+1}]$, multiplying (2.11) by $\overline{E}$, the conjugate of E, we get

$$i\ E_t\ \overline{E} = \alpha N |E|^2 - \lambda |E|^4 - i\gamma |E|^2. \tag{2.12}$$

Then calculating the conjugate of the ODE (2.11) and multiplying it by E, one finds

$$-i\ \overline{E}_t\ E = \alpha N |E|^2 - \lambda |E|^4 + i\gamma |E|^2. \tag{2.13}$$

Subtracting (2.13) from (2.12) and then multiplying both sides by $-i$, one gets

$$\frac{d}{dt}(|E(x,t)|^2) = E_t(x,t)\overline{E(x,t)} + \overline{E_t(x,t)}E(x,t) = -2\gamma |E(x,t)|^2 \tag{2.14}$$

and therefore

$$|E(x,t)|^2 = e^{-2\gamma(t-t_m)} |E(x,t_m)|^2, \quad t_m \le t \le t_{m+1}. \tag{2.15}$$

Substituting (2.15) into (2.11), we obtain

$$i\ E_t(x,t) = \alpha N(x,t)\ E(x,t) - \lambda e^{-2\gamma(t-t_m)} |E(x,t_m)|^2\ E(x,t) - i\gamma\ E(x,t). \tag{2.16}$$

Integrating (2.16) from t_m to t_{m+1}, and then approximating the integral of N on $[t_m, t_{m+1}]$ via the trapezoidal rule, one obtains

$$\begin{aligned} E(x, t_{m+1}) &= e^{-i\int_{t_m}^{t_{m+1}} [\alpha N(x,\tau) - \lambda e^{-2\gamma(\tau - t_m)} |E(x,t_m)|^2 - i\gamma]\ d\tau}\ E(x, t_m) \\ &\approx \begin{cases} e^{-ik[\alpha(N(x,t_m)+N(x,t_{m+1}))/2 - \lambda |E(x,t_m)|^2]}\ E(x,t_m), & \gamma = 0, \\ e^{-\gamma k - i[k\alpha(N(x,t_m)+N(x,t_{m+1}))/2 + \lambda |E(x,t_m)|^2 (e^{-2\gamma k}-1)/2\gamma]}\ E(x,t_m), & \gamma \neq 0. \end{cases} \end{aligned}$$

From time $t = t_m$ to $t = t_{m+1}$, we combine the splitting steps via the standard Strang splitting:

$$\varepsilon^2 \frac{N_j^{m+1} - 2N_j^m + N_j^{m-1}}{k^2} - \left(D_{xx}^f N^m - \nu D_{xx}^f |E^m|^2 \right)\Big|_{x=x_j} = 0, \tag{2.17}$$

$$E_j^* = \sum_{l=-M/2}^{M/2-1} e^{-ik\mu_l^2/2} (\widehat{E^m})_l \, e^{i\mu_l (x_j - a)},$$

$$E_j^{**} = \begin{cases} e^{-ik[\alpha(N_j^m + N_j^{m+1})/2 - \lambda |E_j^*|^2]} \, E_j^*, & \gamma = 0, \\ e^{-\gamma k - i[k\alpha(N_j^m + N_j^{m+1})/2 + \lambda |E_j^*|^2 (e^{-2\gamma k} - 1)/2\gamma]} \, E_j^*, & \gamma \neq 0, \end{cases}$$

$$E_j^{m+1} = \sum_{l=-M/2}^{M/2-1} e^{-ik\mu_l^2/2} (\widehat{E^{**}})_l \, e^{i\mu_l (x_j - a)}, 0 \leq j \leq M-1, m = 0, 1, \cdots; \tag{2.18}$$

where $(\widehat{U})_l$, the Fourier coefficients of a vector $U = (U_0, U_1, U_2, \cdots, U_M)^T$ with $U_0 = U_M$, are defined as

$$\mu_l = \frac{2\pi l}{b-a}, \qquad (\widehat{U})_l = \frac{1}{M} \sum_{j=0}^{M-1} U_j \, e^{-i\mu_l (x_j - a)}, \qquad l = -\frac{M}{2}, \cdots, \frac{M}{2} - 1, \tag{2.19}$$

and D_{xx}^f, a spectral differential operator approximation of ∂_{xx}, is defined as

$$D_{xx}^f U \Big|_{x=x_j} = - \sum_{l=-M/2}^{M/2-1} \mu_l^2 (\widehat{U})_l \, e^{i\mu_l (x_j - a)}. \tag{2.20}$$

The initial conditions (2.3) are discretized as

$$E_j^0 = E^0(x_j), \; N_j^0 = N^0(x_j), \; \frac{N_j^1 - N_j^{-1}}{2k} = N_j^{(1)}, \quad j = 0, 1, 2, \cdots, M-1, \tag{2.21}$$

where

$$N_j^{(1)} = \begin{cases} N^{(1)}(x_j), & 0 \leq j \leq M-2, \\ - \sum_{l=0}^{M-2} N^{(1)}(x_l), & j = M-1. \end{cases} \tag{2.22}$$

This type of discretization for the initial condition (2.3) is equivalent to the use of the trapezoidal rule for the periodic function $N^{(1)}$. The discretization error converges to 0 exponentially fast as the mesh size h goes to 0.

Note that the spatial discretization error of the method is of spectral-order accuracy in h and time discretization error is of second-order accuracy in k, which will be demonstrated in section 3 from our numerical results.

If the initial data in (2.3) is chosen as

$$E^0(x) = c \, e^{i2\pi l x/(b-a)}, \qquad N^0(x) = d, \qquad N^{(1)}(x) = 0, \qquad a \leq x \leq b, \tag{2.23}$$

where l is an integer and c, d are constants, then the generalized Zakharov system admits the plane wave solution [27]

$$N(x,t) = d, \qquad a < x < b, \quad t \geq 0, \tag{2.24}$$

$$E(x,t) = \begin{cases} c\, e^{i\left(\frac{2\pi l x}{b-a} - \omega t\right)}, & \omega = \alpha d + \frac{4\pi^2 l^2}{(b-a)^2} - \lambda c^2, \qquad \gamma = 0, \\ c\, e^{-\gamma t} e^{i\left(\frac{2\pi l x}{b-a} - \omega t - \frac{\lambda c^2}{2\gamma}(e^{-2\gamma t}-1)\right)}, & \omega = \alpha d + \frac{4\pi^2 l^2}{(b-a)^2}, \quad \gamma \neq 0. \end{cases} \tag{2.25}$$

It is easy to see that in this case our numerical method TSSP (2.17), (2.18) gives exact results provided that $M \geq 2(|l|+1)$.

Note that a main advantage of the time-splitting spectral method is that if a constant r is added to the initial data $N^0(x)$ in (2.3) when $\gamma = 0$ in (2.1), then the discrete functions N_j^{m+1} obtained from (2.17) get added by r and E_j^{m+1} obtained from (2.18) get multiplied by the phase factor $e^{-ir(m+1)k}$, which leaves the discrete function $|E_j^{m+1}|^2$ unchanged. This property also holds for the exact solution of the ZS, but does not hold for the finite difference schemes proposed in [18, 13] and the spectral method proposed in [28].

Remark 2.1 *If the periodic boundary conditions (2.4) and (2.5) are replaced by (2.9), then the Fourier basis used in the above algorithm can be replaced by the sine basis. In fact, the generalized Zakharov system (2.1) and (2.2) with the homogeneous periodic boundary condition (2.9) and initial condition (2.3) can be discretized by*

$$\varepsilon^2 \frac{N_j^{m+1} - 2N_j^m + N_j^{m-1}}{k^2} - \left(D_{xx}^s N^m - \nu D_{xx}^s |E^m|^2\right)\Big|_{x=x_j} = 0, \tag{2.26}$$

$$E_j^* = \sum_{l=1}^{M-1} e^{-ik\eta_l^2/2} (\widetilde{E^m})_l \, \sin(\eta_l(x_j - a)),$$

$$E_j^{**} = \begin{cases} e^{-ik[\alpha(N_j^m + N_j^{m+1})/2 - \lambda|E_j^*|^2]}\, E_j^*, & \gamma = 0, \\ e^{-\gamma k - i[k\alpha(N_j^m + N_j^{m+1})/2 + \lambda|E_j^*|^2(e^{-2\gamma k}-1)/2\gamma]}\, E_j^*, & \gamma \neq 0, \end{cases}$$

$$E_j^{m+1} = \sum_{l=1}^{M-1} e^{-ik\eta_l^2/2} (\widetilde{E^{**}})_l \, \sin(\eta_l(x_j - a)), 1 \leq j \leq M-1, m = 0, 1, \cdots, \tag{2.27}$$

where $(\widetilde{U})_l$, the sine-transform coefficients of a vector $U = (U_0, U_1, U_2, \cdots, U_M)^T$ with $U_0 = U_M = 0$, are defined as

$$\eta_l = \frac{\pi l}{b-a}, \qquad \widetilde{U}_l = \frac{2}{M} \sum_{j=1}^{M-1} U_j \, \sin(\eta_l(x_j - a)), \qquad l = 1, 2, \cdots, M-1, \tag{2.28}$$

and D_{xx}^s, a spectral differential operator approximating ∂_{xx} based on sine-basis, is defined as

$$D_{xx}^s U|_{x=x_j} = -\sum_{l=1}^{M-1} \eta_l^2 (\widetilde{U})_l \, \sin(\eta_l(x_j - a)). \tag{2.29}$$

Let $U = (U_0, U_1, \cdots, U_M)^T$ with $U_0 = U_M$, $f(x)$ a periodic function on the interval $[a, b]$, and let $\|\cdot\|_{l^2}$ be the usual discrete l^2-norm on the interval (a, b), i.e.,

$$\|U\|_{l^2} = \sqrt{\frac{b-a}{M}\sum_{j=0}^{M-1}|U_j|^2}, \qquad \|f\|_{l^2} = \sqrt{\frac{b-a}{M}\sum_{j=0}^{M-1}|f(x_j)|^2}. \tag{2.30}$$

Then we have

Theorem 2.1 *The time-splitting spectral discretization TSSP (2.17), (2.18) of the generalized ZS possesses the following properties (in fact, they are the discretized version of (2.7) and (2.8)):*

$$\|E^m\|_{l^2}^2 = e^{-2\gamma t_m}\|E^0\|_{l^2}^2 \qquad m = 0, 1, 2, \cdots, \tag{2.31}$$

$$\frac{b-a}{M}\sum_{j=0}^{M-1}\frac{N_j^{m+1} - N_j^m}{k} = 0, \qquad m = 0, 1, 2, \cdots \tag{2.32}$$

and

$$\frac{b-a}{M}\sum_{j=0}^{M-1} N_j^m = \frac{b-a}{M}\sum_{j=0}^{M-1} N_j^0 = \frac{b-a}{M}\sum_{j=0}^{M-1} N^0(x_j), \qquad m = 0, 1, 2, \cdots. \tag{2.33}$$

Proof: See Appendix.

2.2 Discrete singular convolution (DSC-RK4)

In order to solve the generalized ZS by using DSC for spatial derivatives and the fourth-order Runge-Kutta (RK4) for time integration, we rewrite (2.1), (2.2) into the following form:

$$E_t = iE_{xx} - i\alpha NE + i\lambda|E|^2E - \gamma E, \tag{2.34}$$

$$N_t = F, \tag{2.35}$$

$$F_t = \frac{1}{\varepsilon^2}(N_{xx} - \nu(|E|^2)_{xx}). \tag{2.36}$$

Discrete singular convolution (DSC) methods, proposed in [41], provide a general approach for numerical realization of singular integrations. It has been applied to signal processing and numerical solutions to differential equations. By appropriate approximation of a singular kernel, the discrete singular convolution can be an extremely efficient, accurate and reliable algorithm for practical applications. For more detail of the method, please refer to [41]. The DSC algorithm can be realized by using many approximation kernels. Here, we review how to discretize the second

order spatial derivative of a function $u(x)$ by using the regularized Shannon's kernel [41, 45]

$$u_{xx}(x) \approx \sum_{j=-W}^{W} \delta_{h,\sigma}^{(2)}(x - x_j)u(x_j), \tag{2.37}$$

where $2W+1$ is the computational bandwidth, or effective kernel support, which is usually smaller than the whole computational domain, x_j is grid point, and

$$\delta_{h,\sigma}(x) = \frac{\sin(\pi x/h)}{(\pi x/h)} \exp[-x^2/2\sigma^2] \tag{2.38}$$

is the regularized Shannon's kernel, $\delta_{h,\sigma}^{(2)}$ is a symbol for the second order derivative of $\delta_{h,\sigma}(x)$ with respect to x. The detailed expression for $\delta_{h,\sigma}^{(2)}(x)$ can be easily given as:

$$\delta_{h,\sigma}^{(2)}(x) = \begin{cases} \dfrac{-(\pi/h)\sin(\pi x/h)\exp(-x^2/2\sigma^2)}{x} - 2\dfrac{\cos(\pi x/h)\exp(-x^2/2\sigma^2)}{x^2} \\ -2\dfrac{\cos(\pi x/h)\exp(-x^2/2\sigma^2)}{\sigma^2} + 2\dfrac{\sin(\pi x/h)\exp(-x^2/2\sigma^2)}{\pi x^3/h} \\ +\dfrac{\sin(\pi x/h)\exp(-x^2/2\sigma^2)}{\pi\sigma^2 x/h} + \dfrac{x\sin(\pi x/h)\exp(-x^2/2\sigma^2)}{\pi\sigma^4/h}, & x \neq 0, \\ -\dfrac{3+\pi^2\sigma^2/h^2}{3\sigma^2}, & x = 0. \end{cases} \tag{2.39}$$

In our computations, we choose W=50 and $\sigma = 5h$.

Therefore, the second-order derivative of a function $u(x)$ at the grid point $x = x_j$ is approximated by

$$u_{xx}|_{x=x_j} = \sum_{l=-W}^{W} \delta_{h,\sigma}^{(2)}(lh)u_{j+l}, \tag{2.40}$$

and thus we obtain an ordinary differential system for (2.1) and (2.2), then the classical fourth-order Runge-Kutta method (RK4)[30] is used to evaluate E and N at each time step for the time integration.

2.3 Other methods

In order to compare the accuracy and stability, we consider the Fourier pseudospectral (FPS) method proposed in [31] and wavelet-Galerkin (WG) method proposed in [29] and [2] for spatial derivatives, both of which use RK4 for time discretization, as well as the finite difference (FD) method proposed in [13] for Zakharov system.

2.3.1 Fourier pseudospectral method (FPS-RK4)

We consider the numerical approximation of Eqs. (2.34)-(2.36). As reviewed in [20], if $u(x)$ is a sufficiently smooth function of its variables, its spatial derivatives can be evaluated as

$$\left.\frac{d^n u}{dx^n}\right|_{x=x_j} = \sum_{l=-M/2}^{M/2-1} (i\mu_l)^n (\widehat{u})_l \, e^{i\mu_l(x_j-a)}, \tag{2.41}$$

where $(\widehat{u})_l$ is defined as (2.19). This expression constitutes the basis of the Fourier pseudospectral (FPS) method. For the time integration, the classical fourth-order Runge-Kutta method (RK4) is used to evaluate E and N at each time step. Some detail of FPS-RK4 can also be found in [46].

2.3.2 Wavelet-Galerkin method (WG-RK4)

We also try to use the wavelet-Galerkin method to evaluate the spatial derivatives u_{xx}. Using the idea of [29] and [2], the wavelet-Galerkin method entails representing the function u and u_{xx} as expansions of scaling functions at a particular scale J:

$$u(x) = \sum_k \tilde{c}_k 2^{\frac{J}{2}} \phi(2^J x - k), \tag{2.42}$$

$$u_{xx}(x) = \sum_k \tilde{g}_k 2^{\frac{J}{2}} \phi(2^J x - k); \tag{2.43}$$

where $\tilde{c}_k$ and $\tilde{g}_k$ are the wavelet coefficients of u and u_{xx}, respectively, i.e., they define the function in the wavelet space, and the scaling function ϕ is defined by a dilation equation of the form

$$\phi(x) = \sum a_k \phi(2x - k). \tag{2.44}$$

Compactly supported scaling functions, such as those belonging to the Daubechies family of wavelets [16], have a finite number of nonzero filter coefficients a_k. We denote the number of nonzero filter coefficients by L.

We make variable transformation

$$y = 2^J x,$$

then we get

$$U(y) = u(x) = \sum_k c_k \phi(y - k), \qquad c_k = 2^{\frac{J}{2}} \tilde{c}_k, \tag{2.45}$$

$$F(y) = u_{xx}(x) = \sum_k g_k \phi(y - k), \qquad g_k = 2^{\frac{J}{2}} \tilde{g}_k. \tag{2.46}$$

Refer to [2], we can get

$$\mathcal{F}_k(U) = \mathcal{F}_k(F)/\mathcal{F}_k(K_\Omega). \tag{2.47}$$

The notation $\mathcal{F}_k$ is used for the coefficients in the Fourier space, the convolution kernel $K_\Omega = 2^{2J} \cdot(\Omega_0, \Omega_1, \cdots, \Omega_{L-2}, 0, \cdots, 0, \Omega_{2-L}, \cdots, \Omega_{-1})$, where

$$\Omega_l = \int \phi''(y)\phi(y-l)\, dy$$

are the connection coefficients. The method for computing these coefficients was presented in [10]. Conversely, one gets

$$\mathcal{F}_k(F) = \mathcal{F}_k(U) \cdot \mathcal{F}_k(K_\Omega). \tag{2.48}$$

Therefore, in Eqs. (2.34)-(2.36), the spatial derivatives can be evaluated by (2.48) with $h = \frac{1}{2^J}$. For the time integration, we again use the classical fourth-order Runge-Kutta method (RK4). In our computations, we use DAUB12 wavelet basis [10, 16], i.e., L=12.

2.3.3 Finite difference method (FD)

For convenience of the reader, here we also review the finite difference method proposed for the standard ZS [13], i.e., in (2.1)-(2.2) with $\varepsilon = 1$, $\nu = -1$, $\alpha = 1$, $\lambda = 0$ and $\gamma = 0$:

$$\begin{aligned} & i\frac{E_j^{m+1} - E_j^m}{k} + \frac{1}{2}\left(\frac{E_{j+1}^{m+1} - 2E_j^{m+1} + E_{j-1}^{m+1}}{h^2} + \frac{E_{j+1}^m - 2E_j^m + E_{j-1}^m}{h^2}\right) \\ & = \frac{1}{4}(N_j^m + N_j^{m+1})(E_j^{m+1} + E_j^m), \end{aligned} \tag{2.49}$$

$$\begin{aligned} & \frac{N_j^{m+1} - 2N_j^m + N_j^{m-1}}{k^2} - (1-2\theta)\frac{N_{j+1}^m - 2N_j^m + N_{j-1}^m}{h^2} \\ & -\theta\left(\frac{N_{j+1}^{m+1} - 2N_j^{m+1} + N_{j-1}^{m+1}}{h^2} + \frac{N_{j+1}^{m-1} - 2N_j^{m-1} + N_{j-1}^{m-1}}{h^2}\right) \\ & = \frac{|E_{j+1}^m|^2 - 2|E_j^m|^2 + |E_{j-1}^m|^2}{h^2}. \end{aligned} \tag{2.50}$$

In computations, E_j^0, N_j^0 and N_j^1 are obtained from initial data

$$E_j^0 = E^0(x_j), \qquad N_j^0 = N^0(x_j), \tag{2.51}$$

$$\begin{aligned} N_j^1 = {} & N_j^0 + kN^1(x_j) + \frac{k^2}{2}\left(\frac{N_{j+1}^0 - 2N_j^0 + N_{j-1}^0}{h^2}\right. \\ & \left. + \frac{|E_{j+1}^0|^2 - 2|E_j^0|^2 + |E_{j-1}^0|^2}{h^2}\right). \end{aligned} \tag{2.52}$$

In our computations, we choose either $\theta = 0.5$ or $\theta = 0$.

3 Numerical examples

In this section, we present numerical results of the ZS with a solitary wave solution in 1d to compare the accuracy, stability and ε-resolution of different methods described in section 2. We also present numerical examples including plane waves, soliton-soliton collisions in 1d, as well as a 2d problem of the ZS to demonstrate the efficiency and spectral accuracy of the time-splitting spectral method (TSSP) and discrete singular convolution method (DSC-RK4) for the generalized Zakharov system.

In the examples 1, 3 and 4, the initial conditions for (1.3) are always chosen such that $|E^0|$, N^0 and $N^{(1)}$ decay to zero sufficiently fast as $|\mathbf{x}| \to \infty$. We always compute on a domain, which is large enough such that the periodic boundary conditions do not introduce a significant aliasing error relative to the problem in the whole space.

3.1 Comparisons of different methods

Example 1 The standard ZS with a solitary-wave solution, i.e., we choose $d = 1$, $\alpha = 1$, $\lambda = 0$, $\gamma = 0$ and $\nu = -1$ in (1.1)-(1.3). The well-known solitary-wave solution of the ZS (1.1)-(1.3) in this case is given in [27, 24]

$$E(x,t) = \sqrt{2B^2(1-\varepsilon^2C^2)}\,\mathrm{sech}(B(x-Ct))\; e^{i[(C/2)x-((C/2)^2-B^2)t]}, \tag{3.1}$$

$$N(x,t) = -2B^2\,\mathrm{sech}^2(B(x-Ct)), \quad -\infty < x < \infty, \quad t \geq 0, \tag{3.2}$$

where B, C are constants. The initial condition is taken as

$$E^0(x) = E(x,0), \quad N^0(x) = N(x,0), \quad N^{(1)}(x,0) = N_t(x,0), \qquad -\infty < x < \infty, \tag{3.3}$$

where $E(x,0)$, $N(x,0)$ and $N_t(x,0)$ are obtained from (3.1), (3.2) by setting $t = 0$.

We present computations for two different regimes of the acoustic speed, i.e. $1/\varepsilon$:

Case I. $O(1)$-acoustic speed, i.e. we choose $\varepsilon = 1$, $B = 1$, $C = 0.5$ in (3.1), (3.2). Here we test the spatial and temporal discretization errors, conservation of the conserved quantities as well as the stability constraint of different numerical methods. We solve the problem on the interval [-32, 32], i.e., $a = -32$ and $b = 32$ with periodic boundary conditions. Let $E_{h,k}$ and $N_{h,k}$ be the numerical solution of (1.1), (1.2) in 1d with the initial condition (3.3) by using a numerical method with mesh size h and time step k. To quantify the numerical methods, we define the error functions as

$$e_1 = \|E(\cdot,t) - E_{h,k}(t)\|_{l^2}, \qquad e_2 = \|N(\cdot,t) - N_{h,k}(t)\|_{l^2},$$

$$e = \frac{\|E(\cdot,t) - E_{h,k}(t)\|_{l^2}}{\|E(\cdot,t)\|_{l^2}} + \frac{\|N(\cdot,t) - N_{h,k}(t)\|_{l^2}}{\|N(\cdot,t)\|_{l^2}} = \frac{e_1}{\|E(\cdot,t)\|_{l^2}} + \frac{e_2}{\|N(\cdot,t)\|_{l^2}}$$

and evaluate the conserved quantities by using the numerical solution (i.e., replacing E and N by their numerical counterparts $E_{h,k}$ and $N_{h,k}$, respectively) as

$$
\begin{aligned}
D &= \int_{-\infty}^{\infty} |E(x,t)|^2 \, dx, \\
P &= \int_{-\infty}^{\infty} \left[\frac{i}{2} (E(x,t)\overline{E_x(x,t)} - \overline{E(x,t)} E_x(x,t)) + N(x,t)V(x,t) \right] \, dx, \\
H &= \int_{-\infty}^{\infty} \left[|E_x(x,t)|^2 + N|E|^2 + \frac{1}{2}N^2 + \frac{1}{2}V(x,t)^2 \right] \, dx,
\end{aligned}
$$

where V is the flux and its value is determined from the continuity equation

$$N_t + V_x = 0. \tag{3.4}$$

First, we test the discretization error in space. In order to do this, we choose a very small time step, e.g., $k = 0.00001$ such that the error from time discretization is negligible comparing to the spatial discretization error, and solve the ZS with different methods under different mesh sizes h. Table 1 lists the numerical errors of e_1 and e_2 at $t = 2.0$ with different mesh sizes h for different numerical methods.

	Mesh	$h = 1.0$	$h = \frac{1}{2}$	$h = \frac{1}{4}$
TSSP	e_1	9.810E-2	1.500E-4	2.286E-9
	e_2	0.143	1.168E-3	2.201E-8
DSC-RK4	e_1	0.151	1.955E-4	3.452E-9
	e_2	0.243	2.347E-3	4.692E-8
WG-RK4	e_1	0.697	1.866E-2	1.403E-5
	e_2	0.968	3.651E-2	5.677E-5
FD	e_1	0.491	0.120	2.818E-2
	e_2	0.889	0.209	4.726E-2

Table 1: Spatial discretization error analysis: e_1, e_2 at time t=2 under $k = 0.00001$.

Secondly, we test the discretization error in time. Table 2 shows the numerical errors of e_1 and e_2 at $t = 2.0$ under different time steps k and mesh sizes h for different numerical methods. For the FD method, due to its second-order convergence rate

	h	Error	$k = 0.01$	$k = 0.0025$	$k = 0.000625$	$k = 0.00015625$
TSSP	$\frac{1}{4}$	e_1	4.631E-5	2.894E-6	1.809E-7	1.148E-8
		e_2	1.029E-4	6.429E-6	4.024E-7	3.338E-8
	$\frac{1}{8}$	e_1	4.631E-5	2.894E-6	1.809E-7	1.129E-8
		e_2	1.029E-4	6.429E-6	4.018E-7	2.513E-8
DSC-RK4	$\frac{1}{4}$	e_1	2.822E-9	3.442E-9	3.452E-9	3.452E-9
		e_2	4.693E-8	4.692E-8	4.692E-8	4.692E-8
	$\frac{1}{8}$	e_1	—	4.338E-12	3.756E-13	3.765E-13
		e_2	—	3.789E-12	6.194E-14	6.276E-14
FPS-Rk4	$\frac{1}{4}$	e_1	2.078E-9	2.185E-9	2.192E-9	2.192E-9
		e_2	5.990E-8	5.989E-8	5.989E-8	5.989E-8
	$\frac{1}{8}$	e_1	—	4.342E-12	7.369E-14	7.218E-14
		e_2	—	3.762E-12	1.467E-14	4.899E-15
WG-RK4	$\frac{1}{4}$	e_1	1.399E-5	1.403E-5	1.403E-5	1.403E-5
		e_2	5.677E-5	5.677E-5	5.677E-5	5.677E-5
	$\frac{1}{8}$	e_1	8.172E-9	8.506E-9	8.508E-9	8.508E-9
		e_2	4.239E-8	4.221E-8	4.221E-8	4.221E-8
	h	Error	$k = 0.8$	$k = 0.2$	$k = 0.05$	$k = 0.0125$
FD	$\frac{1}{4}$	e_1	0.802	3.480E-2	2.855E-2	2.820E-2
		e_2	0.674	9.012E-2	5.005E-2	4.743E-2
	$\frac{1}{8}$	e_1	0.809	1.753E-2	7.363E-3	6.961E-3
		e_2	0.656	5.491E-2	1.427E-2	1.167E-2

Table 2: Time discretization error analysis: e_1, e_2 at time t=2.

in space, we list errors for larger time steps k in order to view the convergence rate in time.

Thirdly, we test the conservation of conserved quantities. Table 3 presents the quantities and numerical errors at different times with mesh size $h = \frac{1}{8}$ and time step $k = 0.001$ for different numerical methods.

Fourthly, we compare the stability constraint for different numerical methods and list the results in Table 4. There the error e is computed at time $t = 5.0$.

	Time	e	D	P	H
TSSP	1.0	5.323E-7	3.0000000000	3.397277646	0.519446033
	2.0	7.127E-7	3.0000000000	3.397277653	0.519446032
DSC-RK4	1.0	1.966E-13	3.0000000000	3.397343618	0.519445999
	2.0	2.813E-13	3.0000000000	3.397343618	0.519445999
FPS-RK4	1.0	9.631E-14	3.0000000000	3.397343618	0.519445999
	2.0	1.184E-13	3.0000000000	3.397343618	0.519445999
WG-RK4	1.0	3.064E-8	3.0000000000	3.397343618	0.51944599
	2.0	2.319E-8	3.0000000000	3.397343618	0.51944599
FD	1.0	4.745E-3	3.0000000000	3.394829741	0.510115589
	2.0	8.983E-3	3.0000000000	3.394791238	0.510076710

Table 3: Conserved quantities analysis: $k = 0.001$ and $h = \frac{1}{8}$.

Case II: 'Subsonic limit' regime, i.e. we choose $\varepsilon \ll 1$, $B = 1$ and $C = 1/2\varepsilon$ in (3.1), (3.2). Here we test the ε-resolution of different numerical methods. We solve the problem on the interval [-8, 120], i.e., $a = -8$ and $b = 120$ with periodic boundary conditions. Figure 1 shows the numerical results of TSSP at $t = 1$ when we choose the meshing strategy: $\varepsilon = \frac{1}{8}$, $h = \frac{1}{2}$, $k = \frac{1}{50}$; $\varepsilon = \frac{1}{32}$, $h = \frac{1}{8}$, $k = \frac{1}{800}$; $\varepsilon = \frac{1}{128}$, $h = \frac{1}{32}$, $k = \frac{1}{12800}$ corresponding to $h = O(\varepsilon)$ and $k = O(\varepsilon h) = O(\varepsilon^2)$. FPS-RK4 gives similar results at the same meshing strategy.

From Tables 1-4 and Figure 1, we can draw the following observations:

h		DSC-RK4	TSSP	FPS-RK4	WG-RK4	FD ($\theta = \frac{1}{2}$)	FD($\theta = 0$)
$\frac{1}{2}$	k	$\frac{1}{16}$	$\frac{1}{4}$	$\frac{1}{16}$	$\frac{1}{8}$	$\frac{1}{2}$	$\frac{1}{2}$
	e	1.125E-3	0.101	1.645E-3	4.388E-2	0.702	0.207
$\frac{1}{4}$	k	$\frac{1}{64}$	$\frac{1}{8}$	$\frac{1}{64}$	$\frac{1}{32}$	$\frac{1}{4}$	$\frac{1}{4}$
	e	2.458E-8	1.466E-2	3.526E-8	4.815E-5	0.167	4.194E-2
$\frac{1}{8}$	k	$\frac{1}{256}$	$\frac{1}{16}$	$\frac{1}{256}$	$\frac{1}{128}$	$\frac{1}{8}$	$\frac{1}{8}$
	e	2.465E-11	3.163E-3	4.936E-11	2.552E-8	3.937E-2	1.009E-2
$\frac{1}{16}$	k	$\frac{1}{1024}$	$\frac{1}{32}$	$\frac{1}{1024}$	$\frac{1}{512}$	$\frac{1}{16}$	$\frac{1}{16}$
	e	2.869E-13	7.812E-4	2.659E-13	9.147E-12	9.758E-3	2.499E-3

Table 4: Stability analysis: e is computed at time $t = 5.0$.

(1) For TSSP, the spatial discretization error is of spectral order accuracy and the time discretization error is of second-order accuracy. TSSP conserves D exactly and P, H very well (up to 8 digits). The stability constraint of TSSP is weaker, it requires $k = O(h)$ for $\varepsilon = O(1)$. Furthermore, it is explicit, easy to program, less memory requirement, easy to extend to 2d and 3d cases and keeps more properties of the generalized ZS in the discretized level.

(2) DSC-RK4 can also obtain the exponentially high order accuracy in space. Table 3 shows that DSC-RK4 can conserve D, P and H very well. The stability constraint of DSC-RK4 is $k = O(h^2)$ for $\varepsilon = O(1)$. Furthermore, DSC-RK4 is explicit and can be applied to deal with complex geometry and more general boundary conditions.

(3) FD, FPS-RK4 and WG-RK4 give good approximations of the standard ZS with the solitary-wave solution. FPS-RK4 and WG-RK4 are explicit and of spectral order accuracy and high order accuracy in space, respectively. The stability constraint of these two methods is $k = O(h^2)$ for $\varepsilon = O(1)$. FD is implicit, time reversible and of second order accuracy in both space and time. The stability constraint of FD is $k = O(h)$ for $\varepsilon = O(1)$.

(4) In the 'subsonic limit' regime, i.e. $0 < \varepsilon \ll 1$, the ε-resolution is: For TSSP, $h = O(\varepsilon)$ and $k = O(\varepsilon h)$; for DSC-RK4, $h = o(\varepsilon)$ and $k = O(\varepsilon h)$ when the bandwidth w in (2.37) is fixed and $h = O(\varepsilon)$ and $k = O(\varepsilon h)$ when $w = O(1/\varepsilon)$; for FPS-RK4, $h = O(\varepsilon)$ and $k = O(\varepsilon h)$; for WG-RK4 and FD: $h = o(\varepsilon)$ and $k = O(\varepsilon h)$.

In general, the numerical study on the standard ZS with periodic boundary condition suggests that TSSP, DSC-RK4 and FPS-RK4 have much better spatial resolution than FD and WG-RK4. It is obvious that TSSP is easy to program and

less memory requirement, keeps more properties of the generalized ZS in discretized level and its stability constraint is weaker, where DSC-RK4 algorithm can be applied for complex geometry and general boundary conditions. For more comprehensive comparisons between the DSC-RK4 and FPS-RK4 for PDEs, we refer to [46]. In summary, for generalized ZS with periodic boundary conditions or in the whole space with initial data decaying to zero sufficiently fast as $|\mathbf{x}| \to \infty$ which can be approximated in a bounded domain with periodic boundary conditions, we recommend to use TSSP; for generalized ZS in a complex geometry or with non-periodic boundary conditions, we recommend to use DSC-RK4.

3.2 Applications

Example 2 The standard ZS with a plane-wave solution, i.e., we choose $d = 1$, $\varepsilon = 1$, $\alpha = 1$, $\lambda = 0$, $\gamma = 0$ and $\nu = -1$ in (1.1)-(1.3) and consider the problem on the interval $[a, b]$ with $a = 0$ and $b = 2\pi$. The initial condition is taken as

$$E(x,0) = E^0(x) = e^{i7x},\ N(x,0) = N^0(x) = 1,\ N_t(x,0) = N^{(1)}(x) = 0,\ 0 \le x \le 2\pi. \tag{3.5}$$

It is easy to see that the ZS (2.1), (2.2) with the periodic boundary conditions (2.4), (2.5), and initial condition (3.5) admits the plane wave solution [27]

$$E(x,t) = e^{i(7x-\omega t)}, \qquad \text{with} \quad \omega = 7^2 + 1 = 50, \tag{3.6}$$

$$N(x,t) = 1, \qquad a \le x \le b, \quad t \ge 0. \tag{3.7}$$

We solve this problem by using the time-splitting spectral method (TSSP) on the interval $[0, 2\pi]$ with mesh size $h = \frac{\pi}{8}$ (i.e., 17 grid points in the interval $[0, 2\pi]$) and time step $k = 0.01$. Figure 2 shows the numerical results at $t = 2$ and $t = 4$.

From Figure 2, we can see that the time-splitting spectral method really provides the exact plane-wave solution of the Zakharov system.

Example 3 Periodic soliton-soliton collisions in 1d of the standard ZS, i.e., we choose $d = 1$, $\varepsilon = 1$, $\alpha = 1$, $\lambda = 0$, $\gamma = 0$ and $\nu = -1$ in (1.1)-(1.3). The analytic solution of the Zakharov system (2.1)-(2.2), which was derived in [25] and used to test different numerical methods for the ZS in [28, 18, 13]. Here we use this solution to test our method TSSP and DSC-RK4 too. The solution can be written as

$$E_s(x,t;v,E_{\max}) = F(x-vt)\exp[i\phi(x-ut)], \tag{3.8}$$

$$N_s(x,t;v,E_{\max}) = G(x-vt), \tag{3.9}$$

where

$$F(x-vt) = E_{\max}\cdot dn(w,q), \quad G(x-vt) = \frac{|F(x-vt)|^2}{v^2-1} + N_0,$$

$$w = \frac{E_{\max}}{\sqrt{(2(1-v^2))}} \cdot (x - vt), \quad q = \frac{\sqrt{(E_{\max}^2 - E_{\min}^2)}}{E_{\max}},$$
$$\phi = v/2, \qquad \frac{v}{2}L = 2\pi m, \quad m = 1, 2, 3 \cdots, \quad u = \frac{v}{2} + \frac{2N_0}{v} - \frac{E_{\max}^2 + E_{\min}^2}{v(1-v^2)},$$
$$L = \frac{2\sqrt{2(1-v^2)}}{E_{\max}} K(q) = \frac{2\sqrt{2(1-v^2)}}{E_{\max}} K'\left(\frac{E_{\min}}{E_{\max}}\right),$$

with $dn(w,q)$ a Jacobian elliptic function [21, 1], L the period of the Jacobian elliptic functions or the period of the soliton, K and K' the complete elliptic integrals of the first kind [21, 1] satisfying $K(q) = K'\left(\sqrt{1-q^2}\right)$, and N_0 chosen such that $\langle N_s \rangle = \frac{1}{L}\int_0^L N_s(x,t)\ dx = 0$. The values of the various parameters used in our computations are given in Table 5.

Parameter set	L	$E_{\max}$	$E_{\min}$	v	u	N_0
A	160	1.0	1.0535×10^{-31}	0.628319	2.24323	0.0227232
B	160	0.5	1.0535×10^{-18}	0.628319	-0.27094	0.0227232
C	160	1.0	1.0535×10^{-38}	0.314159	-3.22992	0.0227232

Table 5: Parameter values for analytic solutions of the periodic Zakharov system.

In the following we will study soliton-soliton collisions using the time-splitting spectral method. The initial data is chosen as

$$E(x,0) = E_s(x+p, 0, v_1, E_{\max}^1) + E_s(x-p, 0, v_2, E_{\max}^2),$$
$$N(x,0) = N_s(x+p, 0, v_1, E_{\max}^1) + N_s(x-p, 0, v_2, E_{\max}^2),$$
$$N_t(x,0) = \frac{\partial N_s(x+p, 0, v_1, E_{\max}^1)}{\partial t} + \frac{\partial N_s(x-p, 0, v_2, E_{\max}^2)}{\partial t},$$

where $x = \mp p$ are initial locations of the two solitons. We present computations for three cases:

I. Collision of two solutions with equal amplitudes and opposite velocities.

$$E_{\max}^1 = E_{\max}^2 = E_{\max} = 1.0, \qquad v_1 = -v_2 = v = 0.628319, \qquad \text{(parameter set A)}.$$

II. Collision of two solutions with different amplitudes and opposite velocities.

$$E_{\max}^1 = 0.5, \quad v_1 = 0.628319, \qquad \text{(parameter values set B)},$$
$$E_{\max}^2 = 1.0, \quad v_2 = -0.628319, \qquad \text{(parameter values set A)}.$$

III. Collision of two solutions with equal amplitudes and opposite velocities but different speeds.

$$E^1_{\max} = 1.0, \quad v_1 = 0.314159, \qquad \text{(parameter value set C)},$$
$$E^2_{\max} = 1.0, \quad v_2 = -0.628319, \qquad \text{(parameter value set A)}.$$

We solve the problem in the interval $[-80, 80]$, i.e., $a = -80$ and $b = 80$ with mesh size $h = \frac{5}{16}$ and time step $k = 0.01$. We take $p = 10$. Figure 3 shows the values of $|E(x,t)|$ and $N(x,t)$ at various times for case I, Figure 4 for case II and Figure 5 for case III.

Case I which was already used in [28, 13, 18] to test their numerical methods corresponds to collision of two solutions with equal amplitudes and opposite velocities. In this case, the time $t = 15.9$ corresponds to the time when the two solutions are at the same position and the time $t = 31.8$ corresponds to a time when the collision is nearing completion (cf. Figure 3). From the figure we can see that during the collision waves are emitted, and that after the collision the two solutions have a reduced value of $E_{\max}$. Comparison of our graphical results (under mesh size $h = \frac{5}{16}$) with those (under mesh size $h = \frac{1}{20}$) of [28, 18, 13] shows excellent qualitative agreement. This also demonstrates that the time-splitting spectral method TSSP has a better resolution than the finite difference method proposed in [18, 13]. Case II corresponds to the collision of a right-going soliton with a smaller peak value of $E^1_{\max}$ and a left-going soliton with a larger value of $E^2_{\max}$. They have equal speeds. In this case, during the collision waves are emitted and exchanged, and that after the collision the peak value of the left-going soliton becomes bigger than its value before collision and the peak of the other becomes much smaller (cf. Figure 4). This means that the soliton with larger peak value will absorb part of the other wave during their collision. Case III corresponds to a collision of a right-going soliton with a smaller speed $|v_1|$ and a left-going soliton with a larger speed $|v_2|$. They have equal amplitudes. Again, waves are emitted and exchanged during collision. After the collision, the peak value of the left-going soliton becomes larger than its value before collision and the peak of the other becomes much smaller (cf. Figure 5). This means that the soliton with larger speed will absorb part of the other wave during their collision.

The same results can also be obtained by the DSC-RK4 with mesh size $h = \frac{5}{16}$ and time step $k = 0.01$.

Example 4 A 2d problem of the standard ZS, i.e., we choose $d = 2$, $\varepsilon = 1$, $\alpha = 1$, $\lambda = 0$, $\gamma = 0$ and $\nu = -1$ in (1.1)-(1.3). The initial condition is taken as

$$E(x,y,0) = \frac{2}{e^{x^2+2y^2} + e^{-(x^2+2y^2)}}\, e^{i5/\cosh(\sqrt{4x^2+y^2})},$$
$$N(x,y,0) = e^{-(x^2+y^2)}, \qquad N_t(x,y,0) = 0.$$

We solve the problem on the rectangle $[-64, 64]^2$ with mesh size $h = \frac{1}{4}$ and time step $k = 0.01$. Figure 6 shows the surface plots of $|E|^2$ and N at time $t = 2.0$, as well as the contour plots of $|E|^2$ and N at different times.

From Figure 6, we can see that the time-splitting spectral method can really be applied to solve 2d Zakharov system.

Example 5 Soliton-soliton collisions in 1d of the generalized ZS, i.e., we choose $d = 1$, $\varepsilon = 1$, $\alpha = -2$ and $\gamma = 0$ in (1.1)-(1.3). We use the family of one-soliton solutions in [23] to test our methods TSSP and DSC-RK4. The solution can be written as

$$E_s(x,t;\eta,V) = \left[\frac{\lambda}{2} + \frac{\nu}{\varepsilon^2}(1/\varepsilon^2 - V^2)^{-1}\right]^{-1/2} U_s, \tag{3.10}$$

$$U_s \equiv 2i\eta \,\mathrm{sech}[2\eta(X - Vt)] \exp\left[iVX/2 + i(4\eta^2 - V^2/4)t + i\Phi_0\right], \tag{3.11}$$

$$N_s(x,t;\eta,V) = \frac{\nu}{\varepsilon^2}(1/\varepsilon^2 - V^2)^{-1}|E_s|^2, \tag{3.12}$$

where η and V being the soliton's amplitude and velocity, and Φ_0 being a trivial phase constant. The initial data is chosen as

$$\begin{aligned} E(x,0) &= E_s(x+p,0,\eta_1,V_1) + E_s(x-p,0,\eta_2,V_2),\\ N(x,0) &= N_s(x+p,0,\eta_1,V_1) + N_s(x-p,0,\eta_2,V_2),\\ N_t(x,0) &= \frac{\partial N_s(x+p,0,\eta_1,V_1)}{\partial t} + \frac{\partial N_s(x-p,0,\eta_2,V_2)}{\partial t}, \end{aligned}$$

where $x = \mp p$ are initial locations of the two solitons.

In all the numerical simulations reported in this example, we set $\lambda = 2$, and $\Phi_0 = 0$. We only simulated the symmetric collisions, i.e., the collisions of solitons with equal amplitudes $\eta_1 = \eta_2 = \eta$ and opposite velocities $V_1 = -V_2 \equiv V$. Here, we present computations for four cases:

I. Collision between solitons moving with the subsonic velocities, $V < 1/\varepsilon = 1$.

$$\begin{aligned} &\text{Case 1:} \quad \nu = 0.2, \quad \eta = 0.3, \quad V = 0.5;\\ &\text{Case 2:} \quad \nu = 2, \quad \eta = 0.3, \quad V = 0.045;\\ &\text{Case 3:} \quad \nu = 2, \quad \eta = 0.3, \quad V = 0.45. \end{aligned}$$

II. Collision between solitons in the transonic regime, $V > 1/\varepsilon = 1$.

$$\text{Case 4:} \quad \nu = 2.0, \quad \eta = 0.3, \quad V = 3.0.$$

We solve the problem on the interval [-128,128], i.e., a = -128 and b = 128 with mesh size $h = \frac{1}{4}$ and time step $k = 0.005$. We take p = 10. Figure 7 shows the evolution of the dispersive wave field $|E|^2$ for case 1, Figure 8 shows the evolutions of the dispersive wave field $|E|^2$ and the acoustic (nondispersive) field N for case 2, Figure 9 for case 3 and Figure 10 for case 4.

Case 1 corresponds to a soliton-soliton collision when the ratio ν/λ is small, i.e., the generalized ZS (2.1), (2.2) is close to the NLS equation. As is seen, the collision seems quite elastic (cf. Figure 7). Case 2 and case 3 correspond to the fusion of the colliding subsonic solitons into the new soliton in the system (2.1), (2.2) at the different velocities. At very small values of V, the collision results in the direct fusion of the colliding solitons into a new solitonlike state, its amplitude and width are almost constant in time (cf. Figure 8). With the growth of V, the appearing soliton demonstrates irregular oscillations in its amplitude and size; the oscillations are accompanied by a conspicuous emission of the acoustic waves (cf. Figure 9). Case 4 corresponds to the collision of two transonic solitons. Note that the emission of the sound waves is inconspicuous at this value of V (cf. Figure 10).

From Figures 6-9, we can see that the time-splitting spectral method can really be applied to solve soliton-soliton collisions of generalized Zakharov system. Furthermore, the DSC-RK4 can also achieve similar results.

4 Conclusions

The time-splitting spectral method (TSSP) and discrete singular convolution method (DSC-RK4) for numerical discretization of the generalized Zakharov system (ZS) are presented. The method of TSSP is explicit, easy to extend to high dimensions, easy to program, less memory requirement, weaker stability constraint, and time reversible and time transverse invariant if the generalized ZS is so. Furthermore it keeps the same decay rate of the wave energy in the generalized ZS, and gives exact results for plane-wave solutions of ZS. Numerical results for a solitary wave solution demonstrate that the method is of spectral-order accuracy in space and second-order accuracy in time as well as 'good' ε-resolution in the 'subsonic limit' regime, i.e. $0 < \varepsilon \ll 1$. The method is applied successfully to simulate soliton-soliton collisions of the (generalized) ZS as well as a 2d problem. Numerical results demonstrate the efficiency and high accuracy of TSSP for these problems.

FPS-RK4 and DSC-RK4 are of spectral accuracy in space and explicit 4th order accuracy in time. Both methods are found to perserve the first few conserved physical quantities to at least 10 digits. Numerical experiments indicate that these two methods perform much better than the WG-RK4 and FD in terms of accuracy, but have a stronger requirement for time integration stability. However, as a local spectral method, the DSC based method can be applied to deal with complex geometry and general (complicated) boundary conditions at spectral accuracy.

In summary, for generalized ZS with periodic boundary conditions or in the whole space with initial data decaying to zero sufficiently fast as $|\mathbf{x}| \to \infty$ which can be approximated in a bounded domain with periodic boundary conditions, we recommend to use TSSP; for generalized ZS in a complex geometry or with non-periodic boundary conditions, we recommend to use DSC-RK4.

Appendix

Proof of Theorem 2.1: From (2.18) in the scheme TSSP, noting (2.30), (2.19), one has

$$\begin{aligned}
\frac{M}{b-a}\|E^{m+1}\|_{l^2}^2 &= \sum_{j=0}^{M-1}\left|E_j^{m+1}\right|^2 = \sum_{j=0}^{M-1}\left|\sum_{l=-M/2}^{M/2-1} e^{-ik\mu_l^2/2}(\widehat{E^{**}})_l\ e^{i\mu_l(x_j-a)}\right|^2 \\
&= M\sum_{l=-M/2}^{M/2-1}\left|e^{-ik\mu_l^2/2}\ (\widehat{E^{**}})_l\right|^2 = M\sum_{l=-M/2}^{M/2-1}\left|(\widehat{E^{**}})_l\right|^2 \\
&= \frac{1}{M}\sum_{l=-M/2}^{M/2-1}\left|\sum_{j=0}^{M-1} E_j^{**}\ e^{-i\mu_l(x_j-a)}\right|^2 = \sum_{j=0}^{M-1}\left|E_j^{**}\right|^2 \\
&= \begin{cases} \sum_{j=0}^{M-1}\left|e^{-ik[\alpha(N_j^m+N_j^{m+1})/2-\lambda|E_j^*|^2]}\ E_j^*\right|^2, & \gamma=0, \\ \sum_{j=0}^{M-1}\left|e^{-\gamma k-i[k\alpha(N_j^m+N_j^{m+1})/2+\lambda|E_j^*|^2(e^{-2\gamma k}-1)/2\gamma]}\ E_j^*\right|^2, & \gamma\neq 0, \end{cases} \\
&= e^{-2\gamma k}\sum_{j=0}^{M-1}\left|E_j^*\right|^2 = e^{-2\gamma k}\sum_{j=0}^{M-1}\left|\sum_{l=-M/2}^{M/2-1} e^{-ik\mu_l^2/2}(\widehat{E^m})_l\ e^{i\mu_l(x_j-a)}\right|^2 \\
&= e^{-2\gamma k}M\sum_{l=-M/2}^{M/2-1}\left|e^{-ik\mu_l^2/2}(\widehat{E^m})_l\right|^2 = e^{-2\gamma k}M\sum_{l=-M/2}^{M/2-1}\left|(\widehat{E^m})_l\right|^2 \\
&= \frac{e^{-2\gamma k}}{M}\sum_{l=-M/2}^{M/2-1}\left|\sum_{j=0}^{M-1} E_j^m e^{-i\mu_l(x_j-a)}\right|^2 = e^{-2\gamma k}\sum_{j=0}^{M-1}\left|E_j^m\right|^2 \\
&= \frac{Me^{-2\gamma k}}{b-a}\|E^m\|_{l^2}^2 = \cdots = \frac{Me^{-2\gamma t_{m+1}}}{b-a}\|E^0\|_{l^2}^2, \quad m\geq 1. \qquad (4.1)
\end{aligned}$$

Thus the equality (2.31) is proved. Here we use the identities

$$\sum_{j=0}^{M-1} e^{i2\pi(k-l)j/M} = \begin{cases} 0, & k-l\neq nM, \\ M, & k-l=nM, \end{cases} \qquad n \text{ integer} \qquad (4.2)$$

and

$$\sum_{l=-M/2}^{M/2-1} e^{i2\pi(k-j)l/M} = \begin{cases} 0, & k-j\neq nM, \\ M, & k-j=nM, \end{cases} \qquad n \text{ integer.} \qquad (4.3)$$

From the equality (2.17), we have

$$\frac{N_j^{m+1}-N_j^m}{k} - \frac{N_j^m-N_j^{m-1}}{k} = \frac{k}{\varepsilon^2}\ \left(D_{xx}^f N^m - \nu D_{xx}^f|E^m|^2\right)\Big|_{x=x_j}, \quad 0\leq j<M. \qquad (4.4)$$

Summing the above equality for j from 0 to $M-1$, noting (2.20), (2.19) and (4.2), we obtain

$$\begin{aligned}
&\sum_{j=0}^{M-1} \frac{N_j^{m+1}-N_j^m}{k} - \sum_{j=0}^{M-1} \frac{N_j^m - N_j^{m-1}}{k} \\
&= \frac{k}{\varepsilon^2} \sum_{j=0}^{M-1} \left(D_{xx}^f N^m - \nu D_{xx}^f |E^m|^2 \right)\Big|_{x=x_j} \\
&= -\frac{k}{\varepsilon^2} \sum_{j=0}^{M-1} \sum_{l=-M/2}^{M/2-1} \mu_l^2 \left[(\widehat{N^m})_l - \nu (\widehat{|E^m|^2})_l \right] e^{i\mu_l (x_j - a)} \\
&= -\frac{k}{\varepsilon^2} \sum_{j=0}^{M-1} \sum_{l=-M/2}^{M/2-1} \mu_l^2 \left[(\widehat{N^m})_l - \nu (\widehat{|E^m|^2})_l \right] e^{i2\pi lj/M} \\
&= -\frac{k}{\varepsilon^2} \sum_{l=-M/2}^{M/2-1} \mu_l^2 \left[(\widehat{N^m})_l - \nu (\widehat{|E^m|^2})_l \right] \sum_{j=0}^{M-1} e^{i2\pi lj/M} \\
&= 0, \qquad m = 1, 2, \cdots .
\end{aligned} \tag{4.5}$$

By induction, we get

$$\sum_{j=0}^{M-1} \frac{N_j^{m+1}-N_j^m}{k} = \sum_{j=0}^{M-1} \frac{N_j^1 - N_j^0}{k}, \qquad m = 1, 2, \cdots . \tag{4.6}$$

Applying (2.21) into (2.17) with $m = 1$, we have

$$\frac{N_j^1 - N_j^0}{k} = N_j^{(1)} + \frac{k}{2\varepsilon^2} \left(D_{xx}^f N^0 - \nu D_{xx}^f |E^0|^2 \right)\Big|_{x=x_j}, \qquad j = 0, 1, 2, \cdots, M. \tag{4.7}$$

Summing (4.7) for j from 0 to $M-1$, noting (2.22) and by proceeding analogously to (4.5), we get

$$\sum_{j=0}^{M-1} \frac{N_j^1 - N_j^0}{k} = \sum_{j=0}^{M-1} N_j^{(1)} + \sum_{j=0}^{M-1} \frac{k}{2\varepsilon^2} \left(D_{xx}^f N^0 - \nu D_{xx}^f |E^0|^2 \right)\Big|_{x=x_j} = 0 + 0 = 0. \tag{4.8}$$

The equality (2.32) is a combination of (4.6) and (4.8). Combining (4.8) and (2.21), we obtain

$$\sum_{j=0}^{M-1} N_j^1 = \sum_{j=0}^{M-1} N_j^0 = \sum_{j=0}^{M-1} N^0(x_j). \tag{4.9}$$

Thus the equality (2.33) is proved from (2.32) by induction and noting (4.9).

Acknowledgment

W.B. acknowledges support by the National University of Singapore grant No. R-151-000-027-112. W.G.W. acknowledges support by the Michigan State University.

References

[1] M. Abramowitz and I.A. Stegun, Handbook of mathematical functions, Dover, New York, (1972).

[2] K. Amaratunga and J. Williams, Wavelet-Galerkin solutions for the one-dimensional partial differential equations, Int. J. Numer. Methods Eng. 37, 2703 (1994).

[3] G. Bao, G.W. Wei and A.H. Zhou, Analysis of regularized Whittaker-Kotel'nikov-Shannon sampling expansion, preprint.

[4] W. Bao, Numerical methods for nonlinear Schrödinger equation under nonzero far-field conditions, preprint.

[5] W. Bao and D. Jaksch, An explicit unconditionally stable numerical method for solving damped nonlinear Schrödinger equations with a focusing nonlinearity, SIAM J. Numer. Anal., to appear.

[6] W. Bao, D. Jaksch and P.A. Markowich, Numerical solution of the Gross-Pitaevskii equation for Bose-Einstein condensation, J. Comput. Phys. 187, 318-342 (2003).

[7] W. Bao, S. Jin and P.A. Markowich, On time-splitting spectral approximations for the Schrödinger equation in the semiclassical regime, J. Comput. Phys. 175, 487 (2002).

[8] W. Bao, S. Jin and P.A. Markowich, Numerical study of time-splitting spectral discretizations of nonlinear Schrödinger equations in the semi-classical regimes, SIAM J. Sci. Comput., to appear.

[9] W. Bao, F.F. Sun, Numerical simulations of the vector Zakharov system for multi-component plasma, preprint.

[10] G. Beylkin, On the representation of operators in bases of compactly supported wavelets, SIAM J. Numer. Anal. 29, 1716 (1992).

[11] J. Bourgain and J. Colliander, On wellposedness of the Zakharov system, Internat. Math. Res. Notices 11, 515 (1996).

[12] C. Canuto, M.Y. Hussaini, A. Quarteroni and T.A. Zhang, Spectral Methods in Fluid Dynamics (Springer-Verlag, New York. 1988).

[13] Q. Chang and H. Jiang, A conservative difference scheme for the Zakharov equations, J. Comput. Phys. 113, 309 (1994).

[14] Q. Chang, B. Guo and H. Jiang, Finite difference method for generalized Zakharov equations, Math. Comp. 64, 537 (1995).

[15] J. Colliander, Wellposedness for Zakharov systems with generalized nonlinearity, J. Diff. Eqs. 148, 351 (1998).

[16] I. Daubechies, Orthonormal bases of compactly supported wavelets, Comm. Pure and Appl. Math. 41, 909 (1988).

[17] B. Fornberg and T.A. Driscoll, A fast spectral algorithm for nonlinear wave equations with linear dispersion, J. Comput. Phys. 155, 456 (1999).

[18] R. Glassey, Approximate solutions to the Zakharov equations via finite differences, J. Comput. Phys. 100, 377 (1992).

[19] R. Glassey, Convergence of an energy-preserving scheme for the Zakharov equations in one space dimension, Math. Comp. 58, 83 (1992).

[20] D. Gottlieb and S.A. Orszag, Numerical analysis of spectral methods (Soc. for Industr. & Appl. Math., Philadelphia, 1977).

[21] I.S. Gradshteyn and I.M. Ryzhik, Table of integrals, series, and products, Academic Press, New York, (1980).

[22] S. Guan, C.-H. Lai and G.W. Wei, Bessel-Fourier analysis of patterns in a circular domain, Physica D. 151, 83 (2001).

[23] H. Hadouaj, B. A. Malomed and G.A. Maugin, Soliton-soliton collisions in a generalized Zakharov system, Phys. Rev. A 44, 3932 (1991).

[24] H. Hadouaj, B. A. Malomed and G.A. Maugin, Dynamics of a soliton in a generalized Zakharov system with dissipation, Phys. Rev. A 44, 3925 (1991).

[25] P.J. Hansen and D.R. Nicholson, Amer. J. Phys. 47, 769 (1979).

[26] R.H. Hardin and F.D. Tappert, Applications of the split-step Fourier method to the numerical solution of nonlinear and variable coefficient wave equations, SIAM Rev. Chronicle 15, 423 (1973).

[27] P.K. Newton, Wave interactions in the singular Zakharov system, J. Math. Phys. 32 (2), 431 (1991).

[28] G.L. Payne, D.R. Nicholson, and R.M. Downie, Numerical solution of the Zakharov equations, J. Comput. Phys. 50, 482 (1983).

[29] S. Qian and J.Weiss, Wavelets and the numerical solution of partial differential equations, J. Comp. Phys. 106(1), 155 (1993).

[30] R.D. Richtmyer and K.W. Morton, Difference methods for initial- value problems, New York (1967).

[31] B.F. Sanders, N.K. Katoposes and J.P. Boyd, Spectral modeling of nonlinear dispersive waves, J. Hydraulic. Eng. ASCE 124, 2 (1998).

[32] L. Schwartz Théore des Distributions (Paris: Hermann), 1951.

[33] E.I. Schulman, Dokl. Akad. Nauk. SSSR 259, 579 [Sov. Phys. Dokl. 26, 691 (1981)].

[34] Z.H. Shao, G.W. Wei and S. Zhao, DSC time-domain solution of Maxwell's equations, J. Comput. Phys., to appear.

[35] G. Strang, On the construction and comparison of differential schemes, SIAM J. Numer. Anal. 5, 506 (1968).

[36] C. Sulem and P.L. Sulem, Regularity properties for the equations of Langmuir turbulence, C. R. Acad. Sci. Paris Sér. A Math. 289, 173 (1979).

[37] F.F. Sun, Numerical studies on the Zakharov system, Master thesis, National University of Singapore, 2003.

[38] T.R. Taha and M.J. Ablowitz, Analytical and numerical aspects of certain nonlinear evolution equations, II. Numerical, nonlinear Schrödinger equation, J. Comput. Phys. 55, 203 (1984).

[39] T.R. Taha and M.J. Ablowitz, Analytical and numerical aspects of certain nonlinear evolution equations, III. Numerical, Korteweg-de Vries equation, J. Comput. Phys. 55, 231 (1984).

[40] D.C. Wan, B.S.V. Patnaik and G.W. Wei, Discrete singular convolution-finite subdomain method for the solution of incompressible viscous flows, J. Comput. Phys. 180, 229 (2002).

[41] G.W. Wei, Discrete singular convolution for the Fokker-Planck equation, J. Chem. Phys. 110, 8930 (1999).

[42] G.W. Wei, A unified approach for solving the Fokker-Planck equation, J. Phys. A. 33, 4935 (2000).

[43] G.W. Wei, Solving quantum eigenvalue problems by discrete singular convolution, J. Phys. B. 33, 343 (2000).

[44] G.W. Wei, Vibration analysis by discrete singular convolution, J. Sound Vibration. 244, 535 (2001).

[45] G.W. Wei, Quasi-wavelets and quasi interpolating wavelets, Chem. Phys. Lett. 296, 215 (1998).

[46] S.Y. Yang, Y.C. Zhou and G.W. Wei, Comparison of the discrete singular convolution algorithm and the Fourier pseudospectral method for solving partial differential equations, Comput. Phys. Commun, 143, 113 (2002).

[47] V.E. Zakharov, Zh. Eksp. Teor. Fiz. 62, 1745 (1972) [Sov. Phys. JETP 35, 908 (1972)].

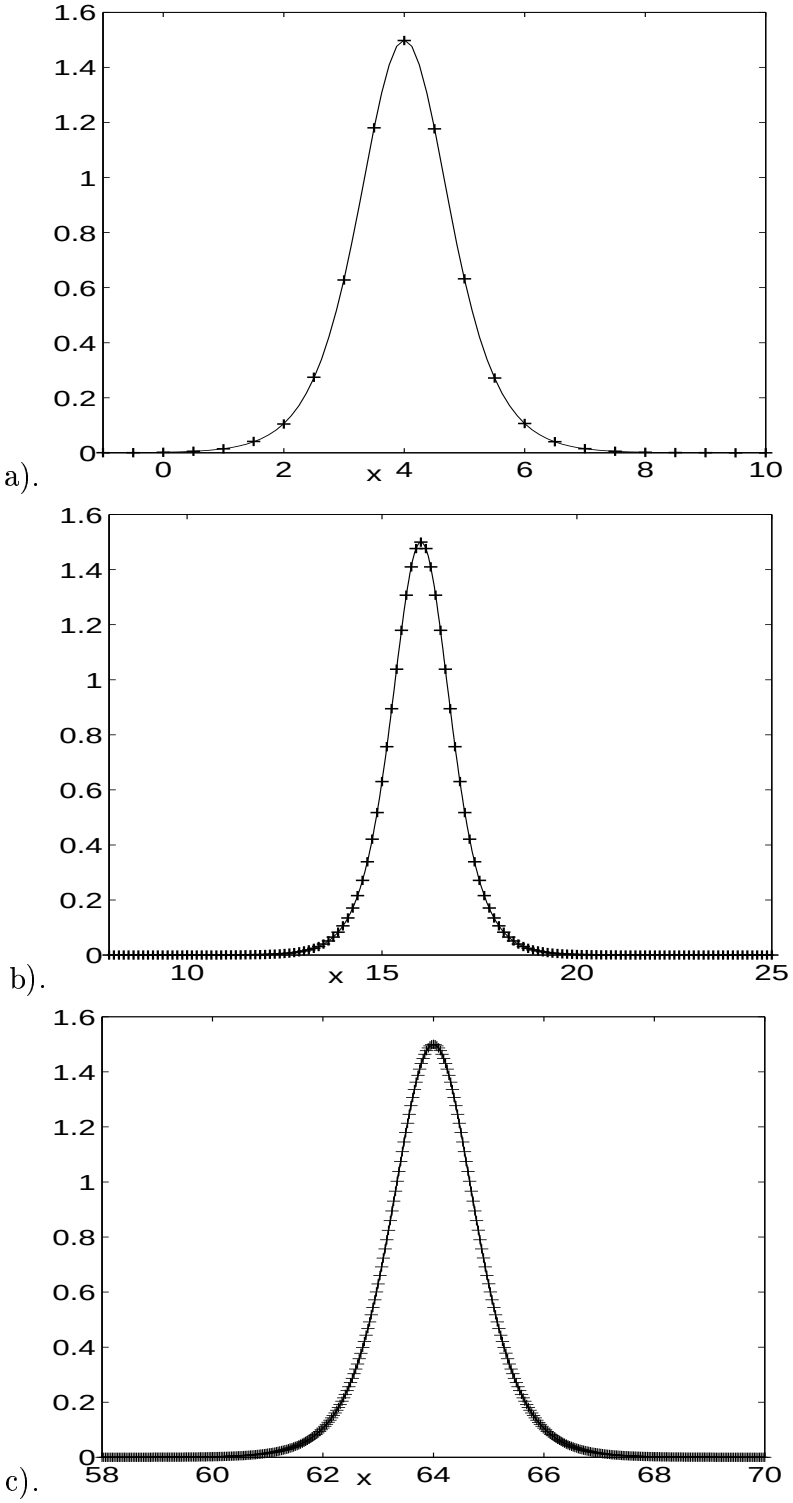

Figure 1: Numerical solutions of the electric field $|E(x,t)|^2$ at $t = 1$ for Example 1 in the 'subsonic limit' regime by TSSP (2.17), (2.18). a). $\varepsilon = \frac{1}{8}$, $h = \frac{1}{2}$, $k = \frac{1}{50}$; b). $\varepsilon = \frac{1}{32}$, $h = \frac{1}{8}$, $k = \frac{1}{800}$; c). $\varepsilon = \frac{1}{128}$, $h = \frac{1}{32}$, $k = \frac{1}{12800}$ corresponding to $h = O(\varepsilon)$ and $k = O(\varepsilon h) = O(\varepsilon^2)$.

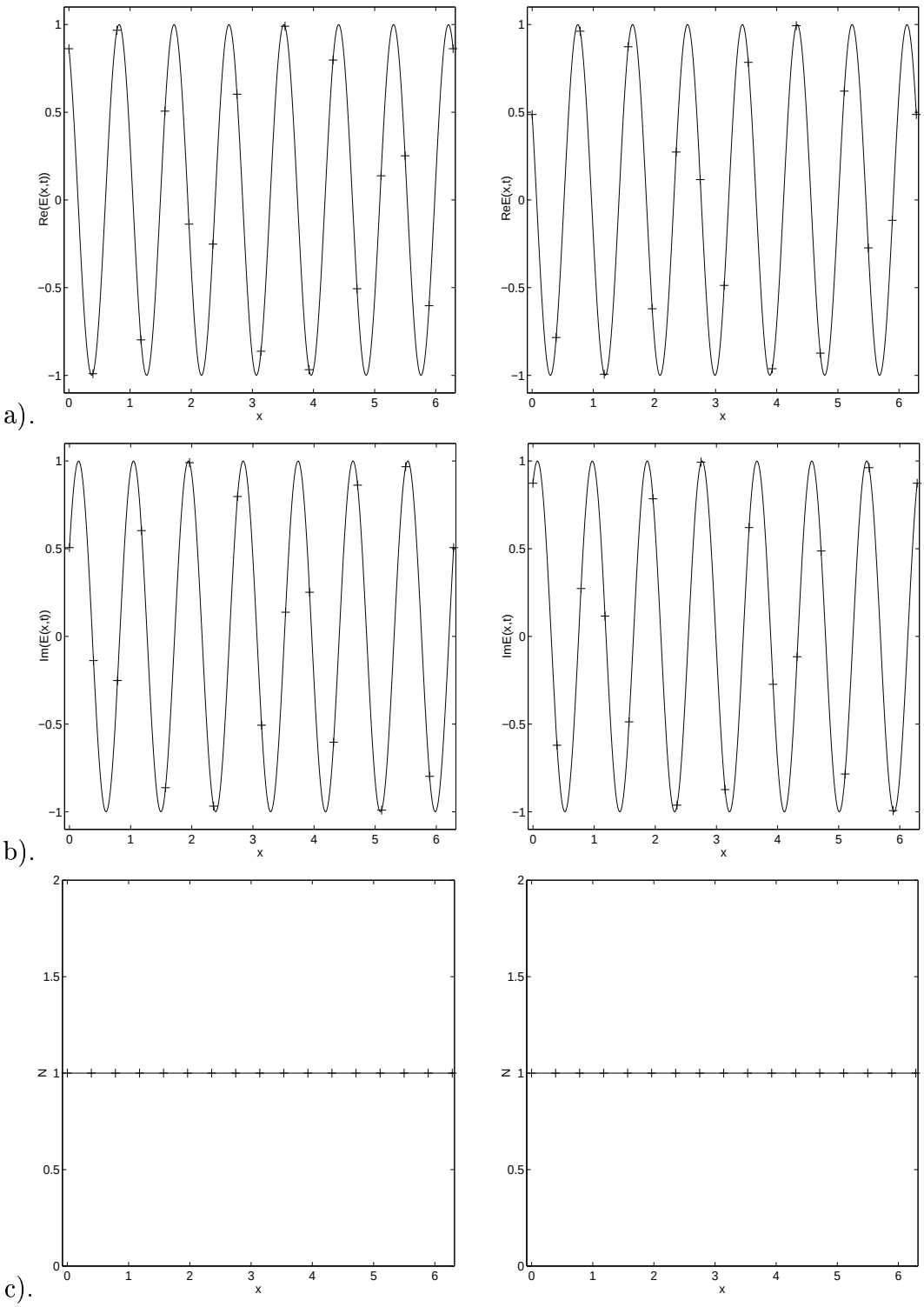

Figure 2: Numerical solutions at $t = 2$ ('left') and $t = 4$ ('right') in Example 1. '—': exact solution given in (3.6)-(3.7), '+ + +': numerical solution. a). $\mathrm{Re}(E(x,t))$: real part of E, b). $\mathrm{Im}(E(x,t))$: imaginary part of E, c). N.

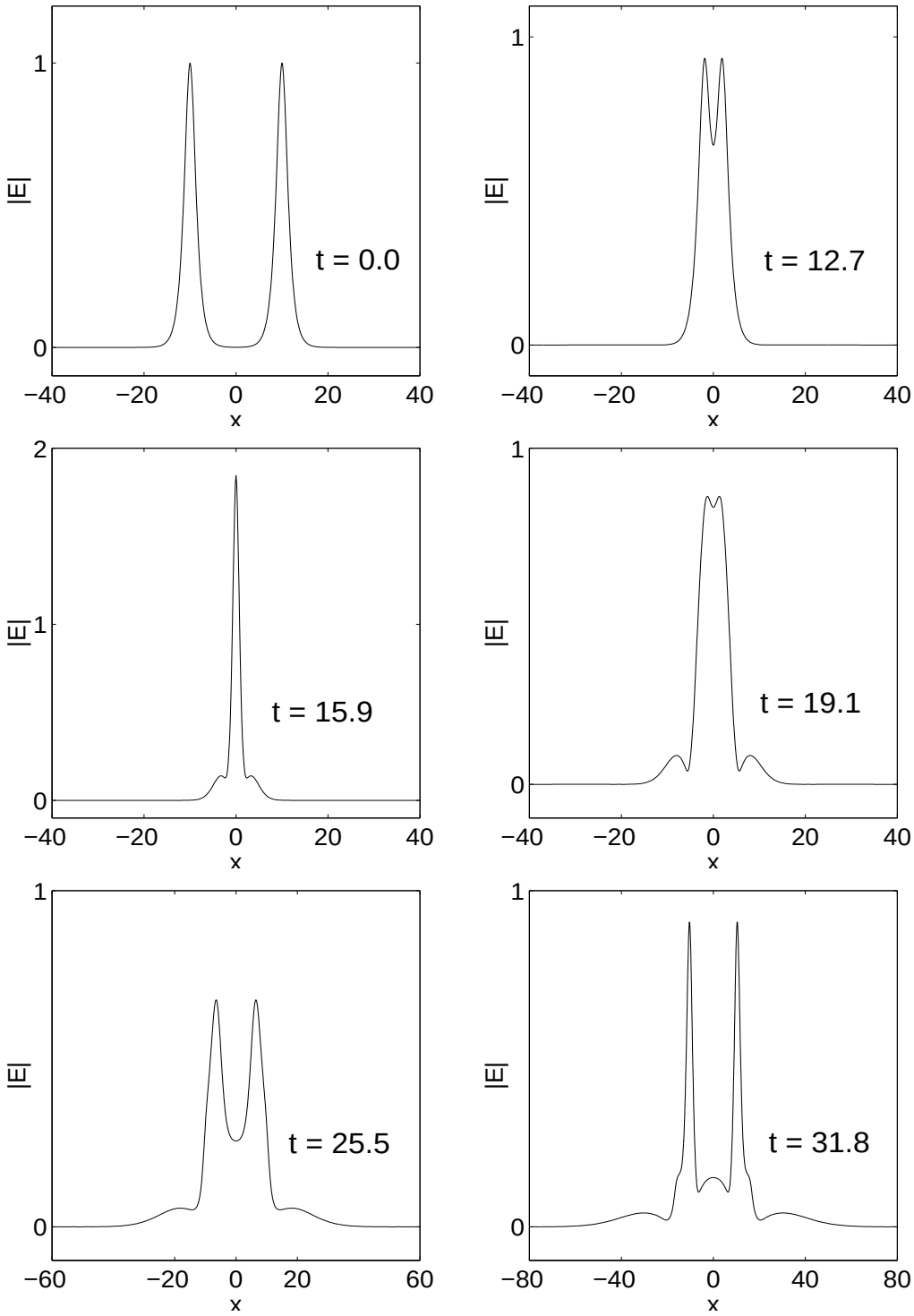

Figure 3: Numerical solutions at different times in Example 3 for case I: Electric field $|E(x,t)|$.

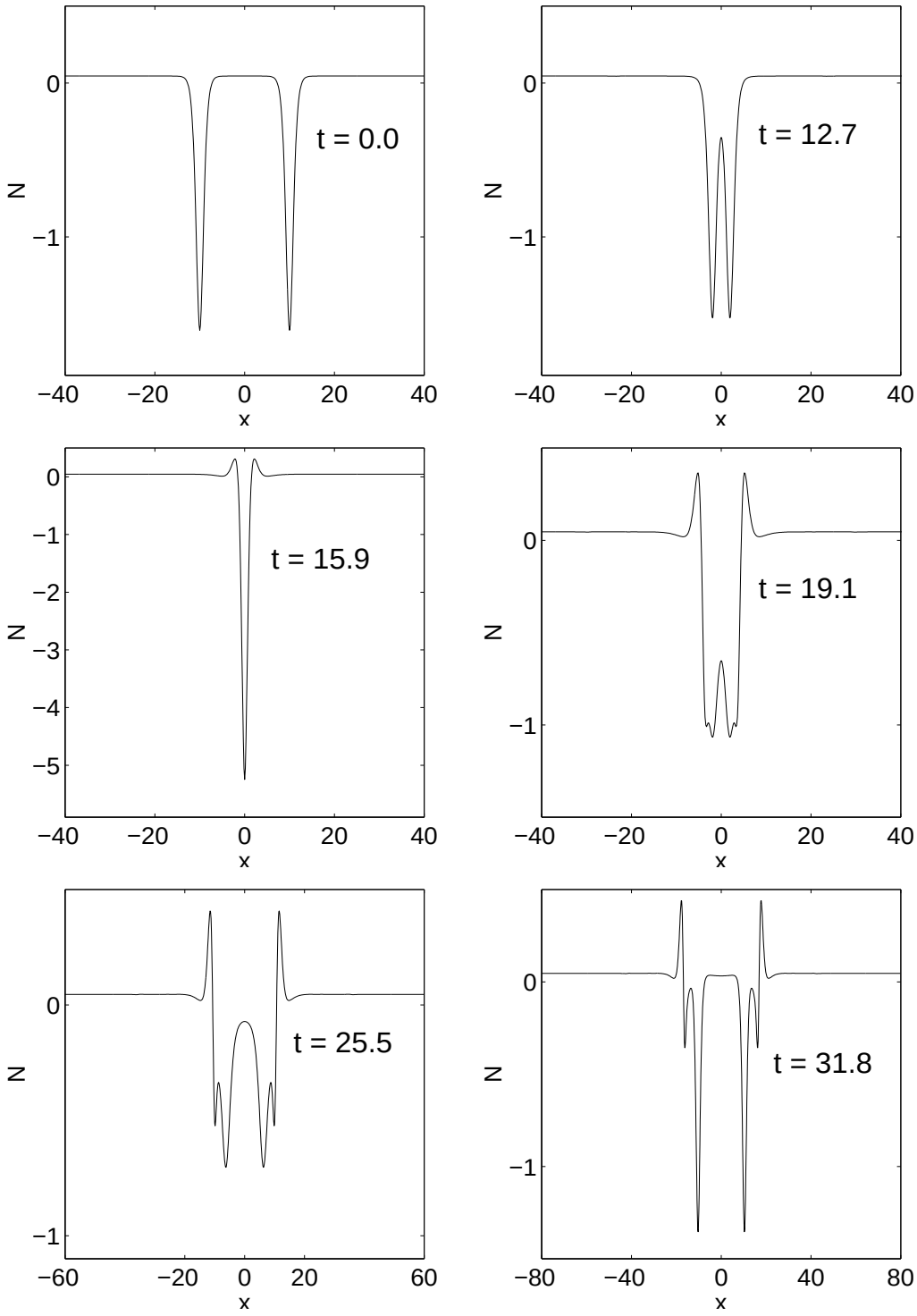

Figure 3 (cont'd): Ion density $N(x,t)$.

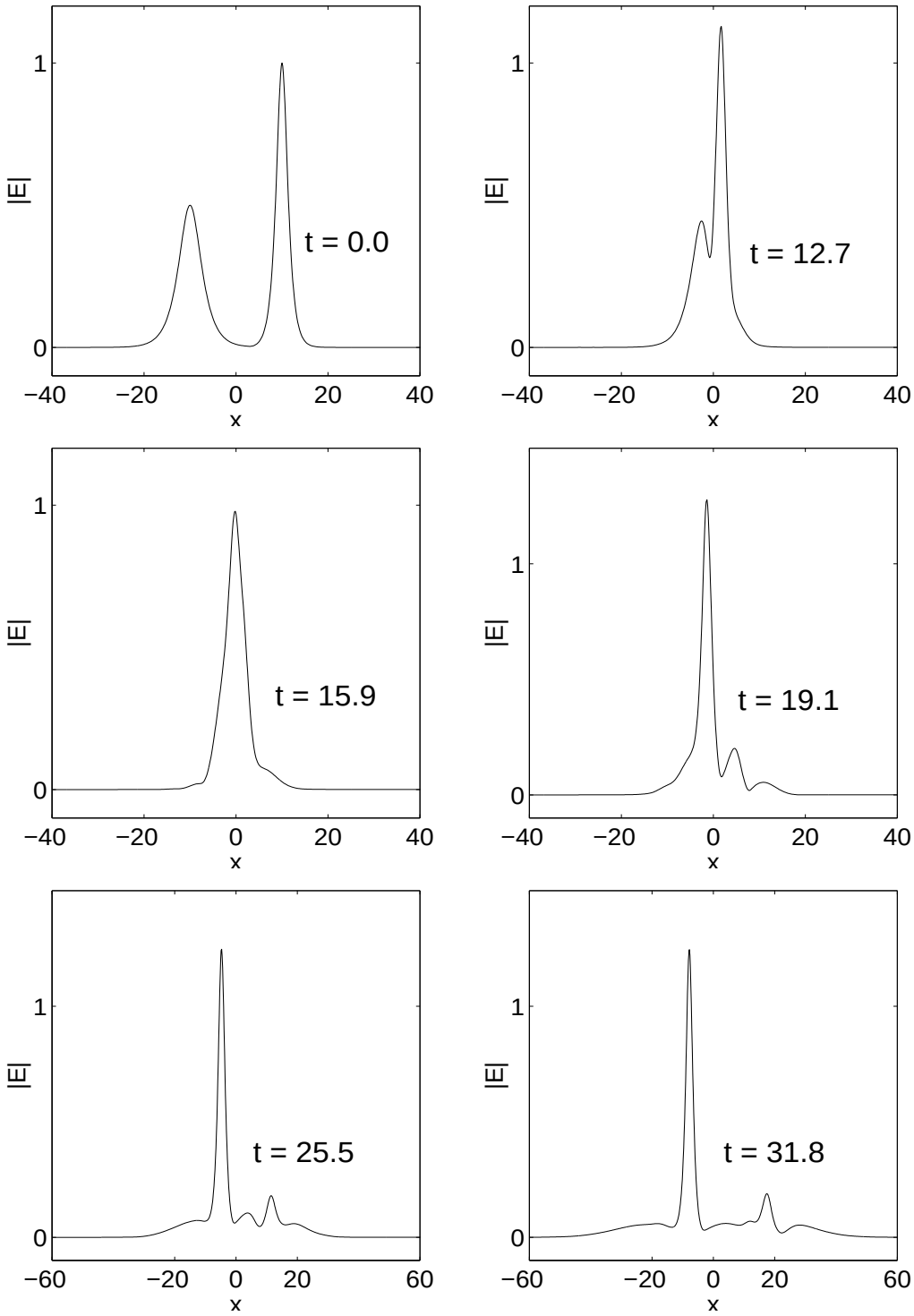

Figure 4: Numerical solutions at different times in Example 3 for case II: Electric field $|E(x,t)|$.

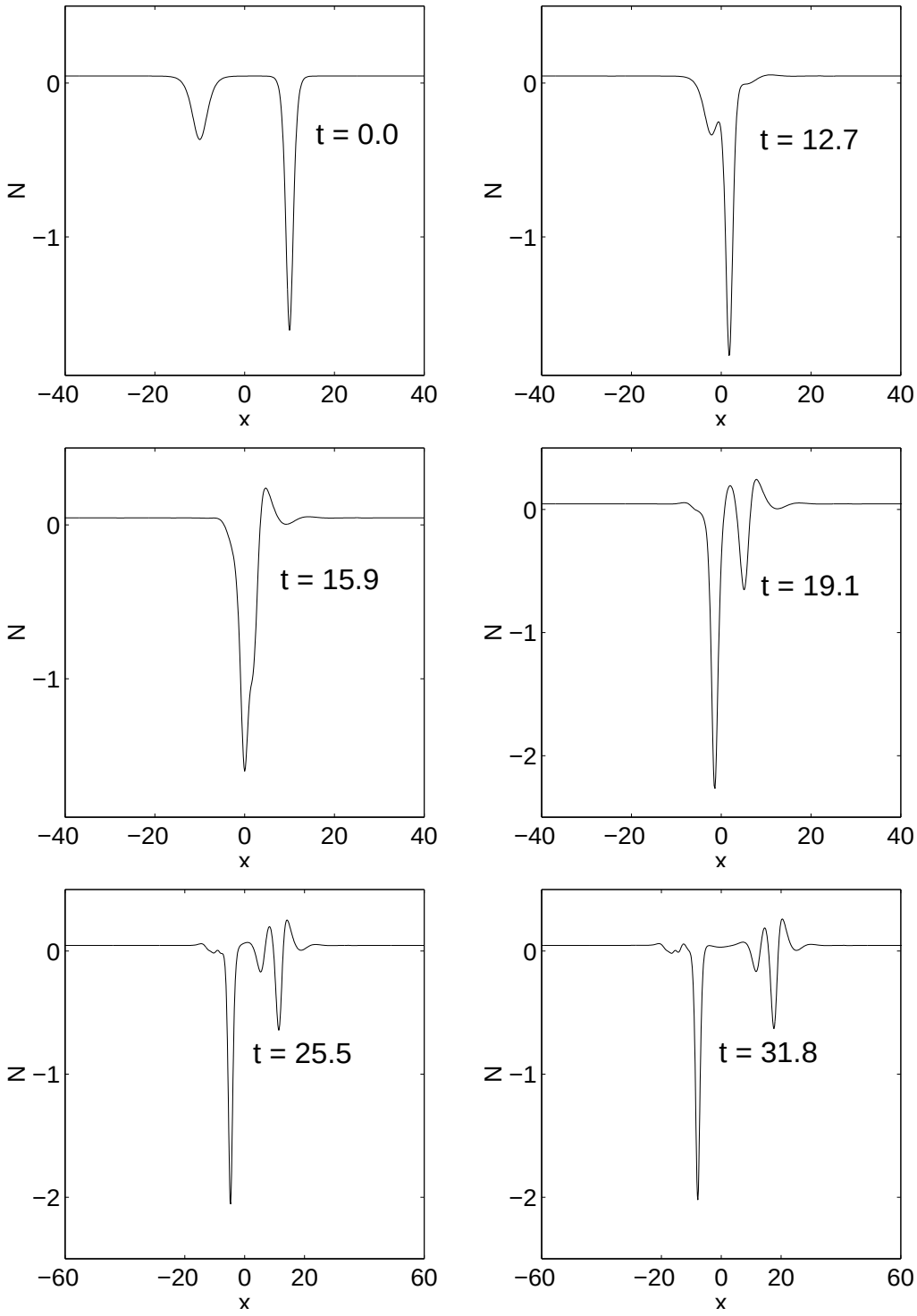

Figure 4 (cont'd): Ion density $N(x,t)$.

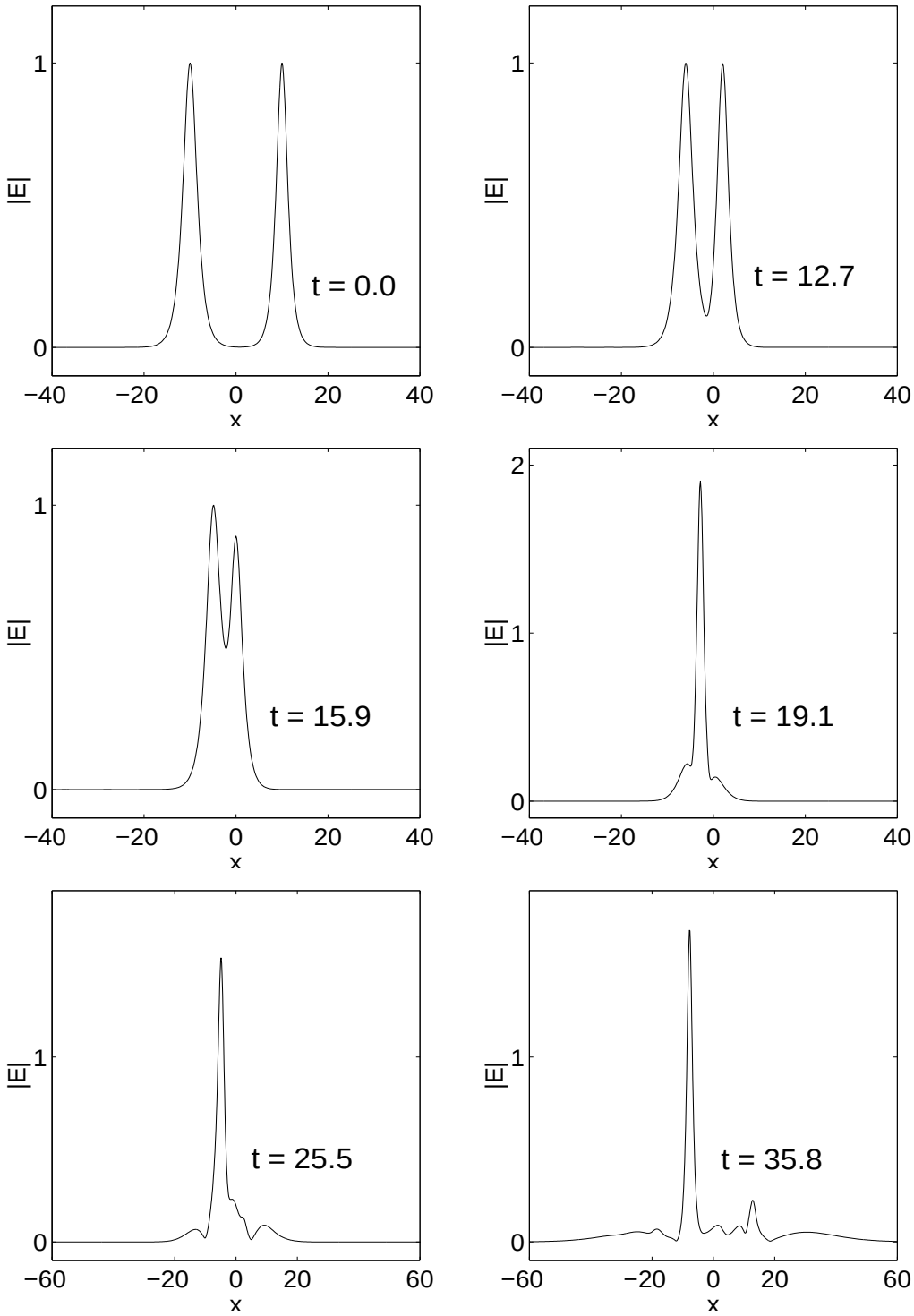

Figure 5: Numerical solutions at different times in Example 3 for case III: Electric field $|E(x,t)|$.

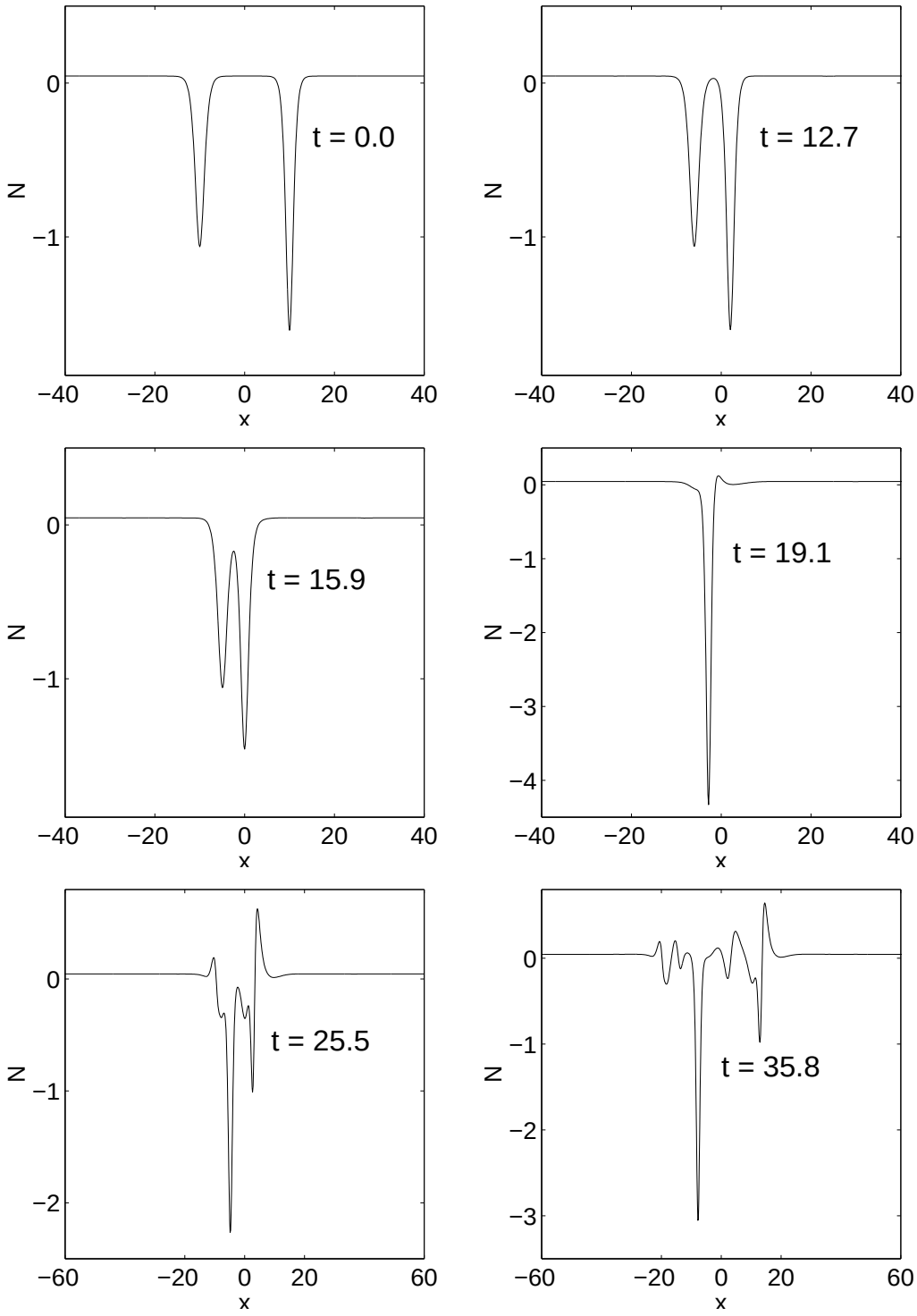

Figure 5 (cont'd): Ion density $N(x,t)$.

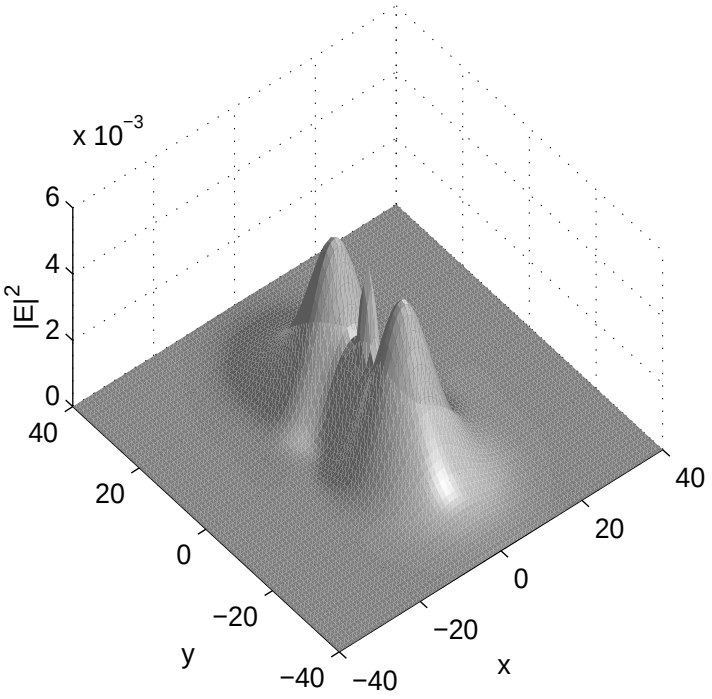

a).

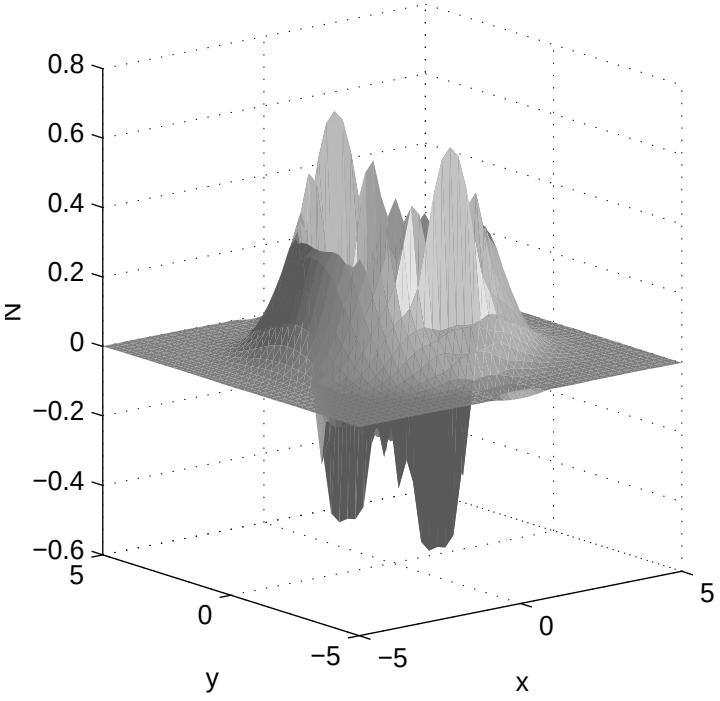

b).

Figure 6: Numerical solutions in Example 4. Surface-plot at time $t = 2.0$: a). Electric field $|E(x, y, 2.0)|^2$, b). Ion density $N(x, y, 2.0)$.

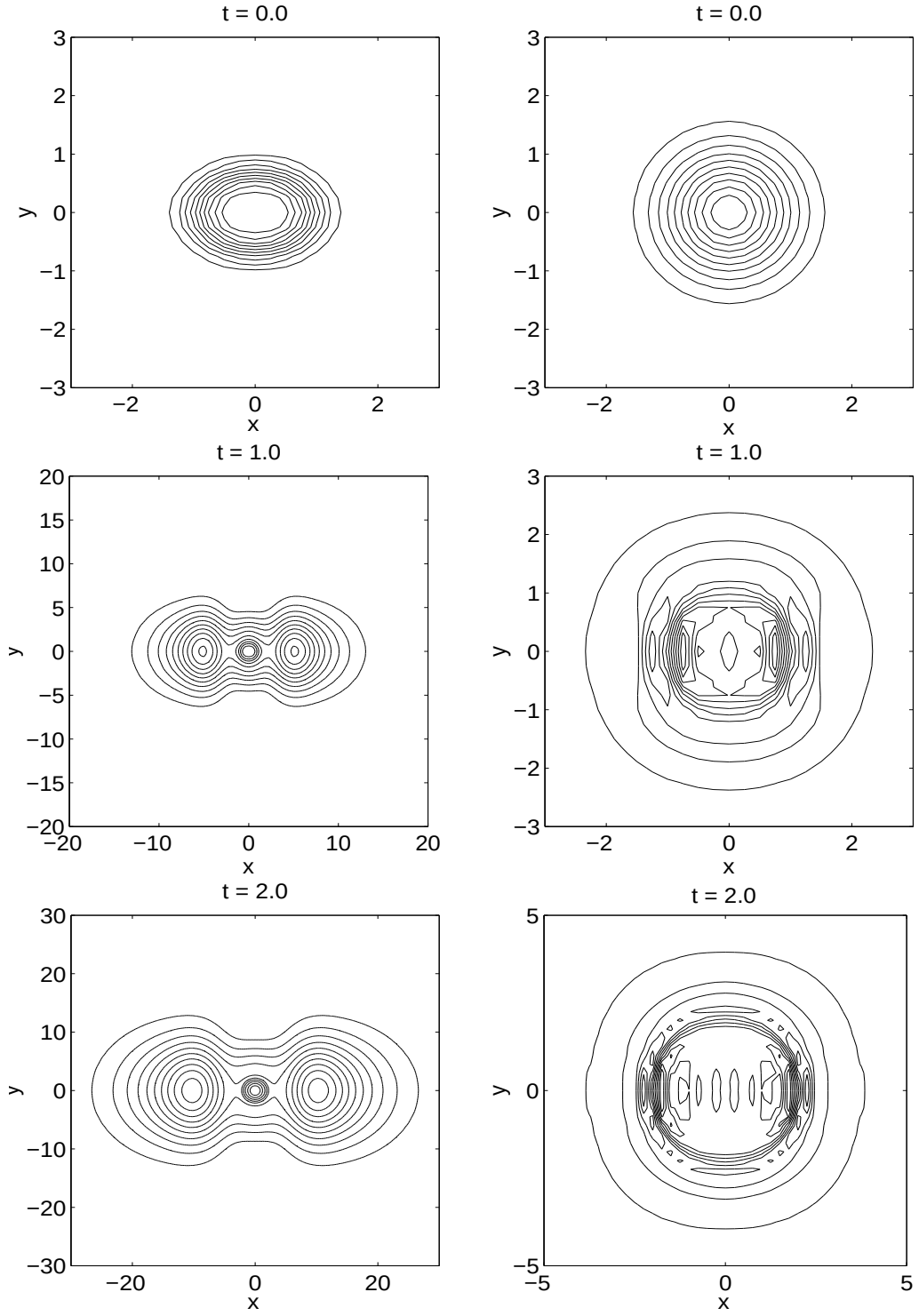

Figure 6 (cont'd): Contour-plots at different times. Left: Electric field $|E|^2$; Right: ion density N.

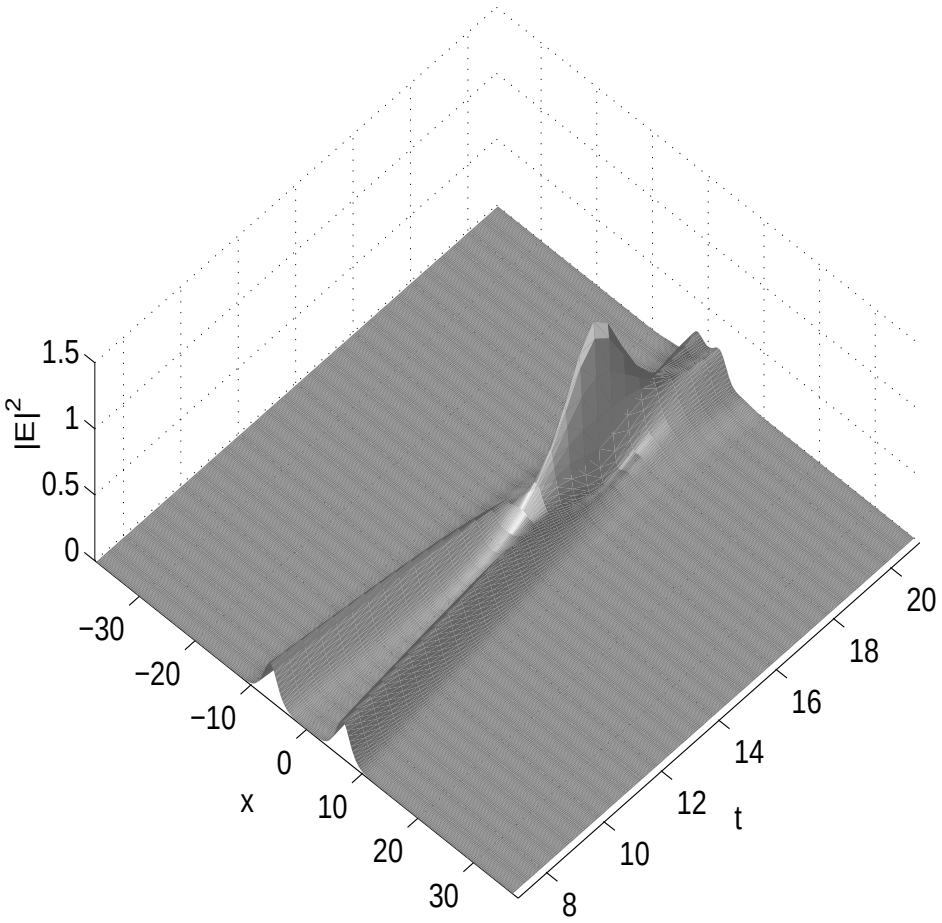

Figure 7: Evolution of the wave field $|E|^2$ in Example 5 for case 1.

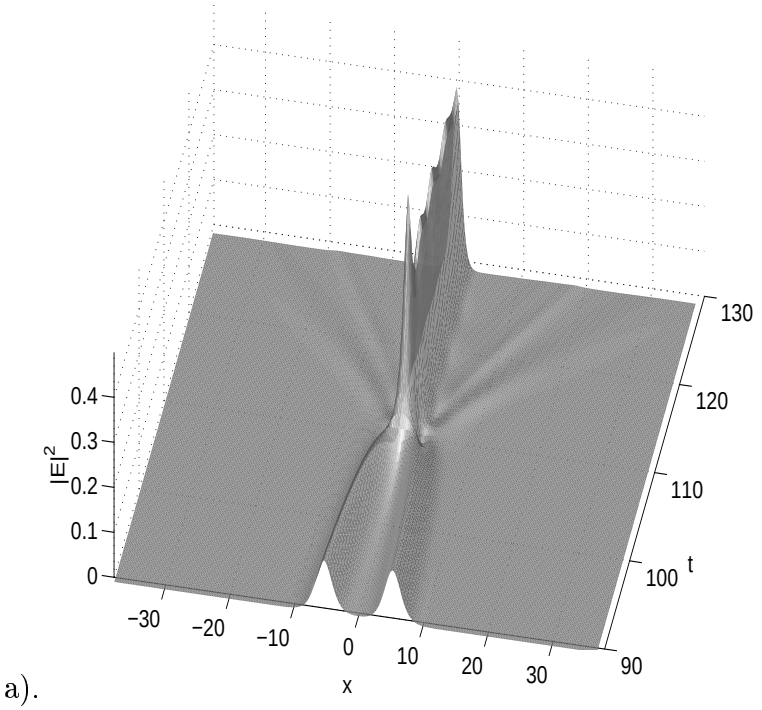

a).

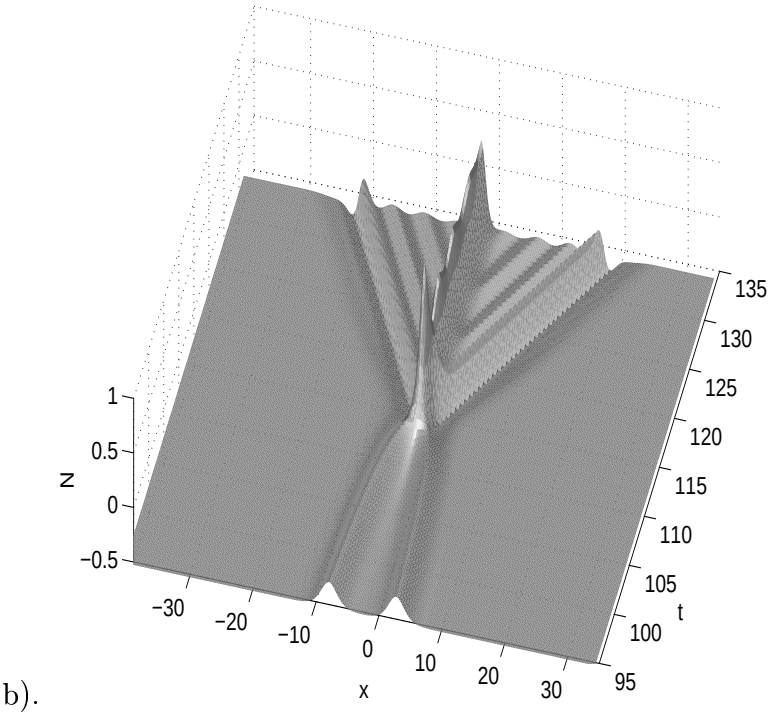

b).

Figure 8: Numerical solutions in Example 5 for case 2. a). Evolution of the wave field $|E|^2$; b). Evolution of the acoustic field N.

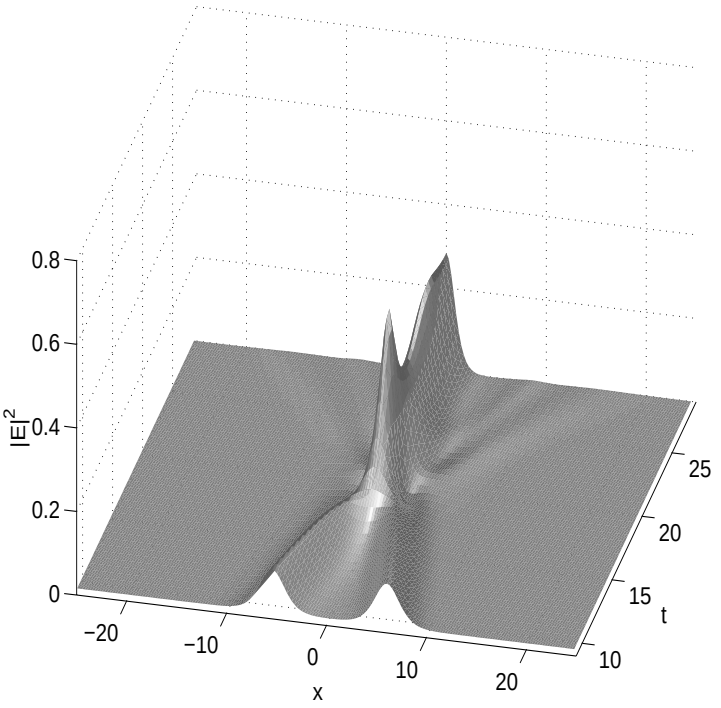

a).

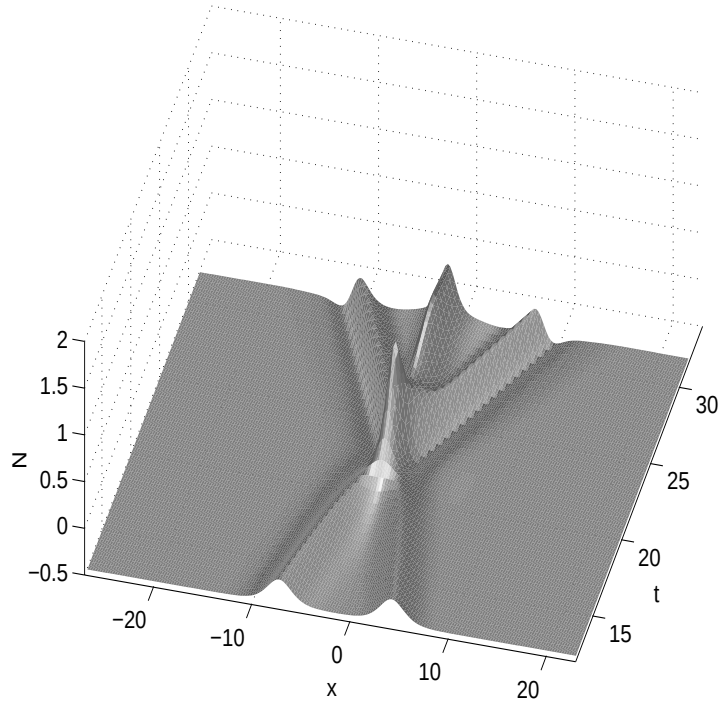

b).

Figure 9: Numerical solutions in Example 5 for case 3. a). Evolution of the wave field $|E|^2$; b). Evolution of the acoustic field N.

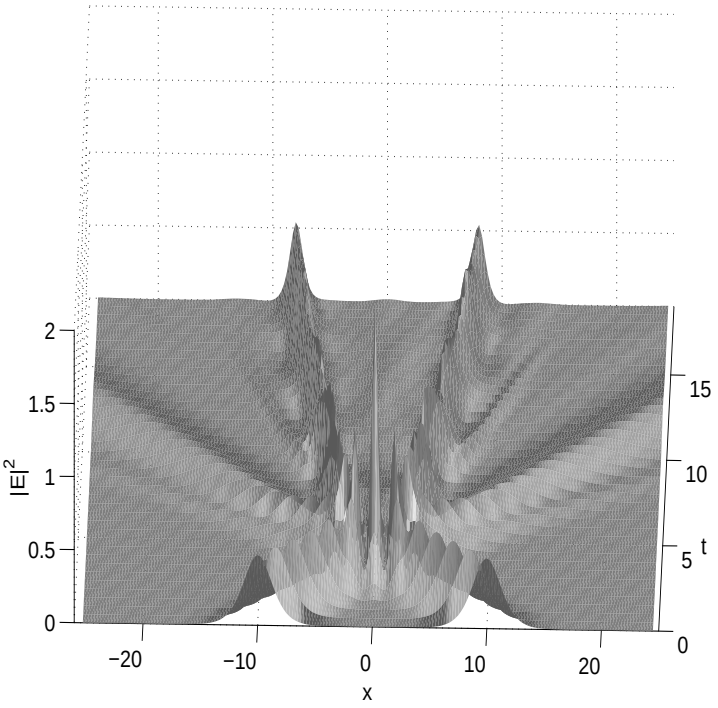

a).

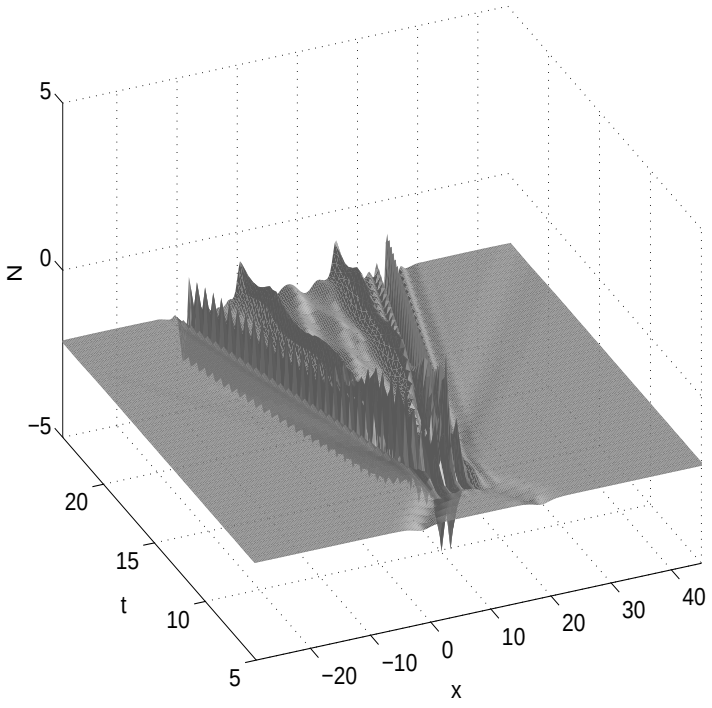

b).

Figure 10: Numerical solutions in Example 5 for case 4. a). Evolution of the wave field $|E|^2$; b). Evolution of the acoustic field N.